Plant Biotechnology Journal
Open Access
aab Association of Applied Biologists
SEB

Plant Biotechnology Journal (2023), pp. 1–16 doi: 10.1111/pbi.14242

A dual-subcellular localized β-glucosidase confers pathogen and insect resistance without a yield penalty in maize

Chuang Liu[1], Shengfeng He[1], Junbin Chen[1], Mingyu Wang[1], Zhenju Li[1], Luyang Wei[1], Yan Chen[1], Meida Du[1], Dandan Liu[1], Cai Li[1], Chunju An[1,2], Vijai Bhadauria[1], Jinsheng Lai[3] and Wangsheng Zhu[1,2,*]

[1]*China Key Laboratory of Pest Monitoring and Green Management, MOA, and College of Plant Protection, China Agricultural University, Beijing, China*
[2]*State Key Laboratory of Maize Bio-breeding, China Agricultural University, Beijing, China*
[3]*State Key Laboratory of Maize Bio-breeding, National Maize Improvement Center, Frontiers Science Center for Molecular Design Breeding, Department of Plant Genetics and Breeding, China Agricultural University, Beijing, China*

Received 18 August 2023;
revised 23 October 2023;
accepted 11 November 2023.
**Correspondence* (Tel +86-10-62734225; fax +86-10-62734225; email wangshengzhu@cau.edu.cn)

Keywords: GWAS, β-glucosidase, broad-spetrcum resistance, maize, natural variation, balanced defense and growth.

Summary

Maize is one of the most important crops for food, cattle feed and energy production. However, maize is frequently attacked by various pathogens and pests, which pose a significant threat to maize yield and quality. Identification of quantitative trait loci and genes for resistance to pests will provide the basis for resistance breeding in maize. Here, a β-glucosidase *ZmBGLU17* was identified as a resistance gene against *Pythium aphanidermatum*, one of the causal agents of corn stalk rot, by genome-wide association analysis. Genetic analysis showed that both structural variations at the promoter and a single nucleotide polymorphism at the fifth intron distinguish the two ZmBGLU17 alleles. The causative polymorphism near the GT-AG splice site activates cryptic alternative splicing and intron retention of ZmBGLU17 mRNA, leading to the downregulation of functional ZmBGLU17 transcripts. ZmBGLU17 localizes in both the extracellular matrix and vacuole and contribute to the accumulation of two defence metabolites lignin and DIMBOA. Silencing of *ZmBGLU17* reduces maize resistance against *P. aphanidermatum*, while overexpression significantly enhances resistance of maize against both the oomycete pathogen *P. aphanidermatum* and the Asian corn borer *Ostrinia furnacalis*. Notably, *ZmBGLU17* overexpression lines exhibited normal growth and yield phenotype in the field. Taken together, our findings reveal that the apoplastic and vacuolar localized *ZmBGLU17* confers resistance to both pathogens and insect pests in maize without a yield penalty, by fine-tuning the accumulation of lignin and DIMBOA.

Introduction

Maize (*Zea mays* L.) is an incredibly versatile crop, serving as a vital source of food, feed, and bio-materials around the world. Despite the steady increase in maize production over recent decades, the impact of pathogens and insects on yield and quality remains a pressing global concern. Worldwide, the estimated loss in maize production due to disease and insect pests is estimated to be around 15% (Mahuku, 2010; Munkvold and White, 2016). Pythium stalk rot, primarily caused by *Pythium* pathogens, is soil-borne disease that is highly damaging to maize production (Duan *et al*., 2019). This disease can occur in various environments but is particularly prevalent in high-humidity conditions, significantly impacting susceptible maize varieties and resulting in substantial declines in both quality and yield (Khokhar *et al*., 2014). In recent years, it has become a predominant maize disease in the Huang-Huai and northwestern regions of China due to changes in climate conditions, cultivation practices, and maize varieties (Duan *et al*., 2019). Chemical and biological means of controlling this disease have yielded limited success (Duan *et al*., 2019), making the identification and utilization of disease-resistant genes for breeding resistant maize varieties the most economically efficient and effective approach to control Pythium stalk rot.

When it comes to fighting off pests and diseases, maize plants have a range of constitutive and inducible defence mechanisms at their disposal (Balmer *et al*., 2013; Chávez-Arias *et al*., 2021). These defences are regulated by plant hormones, including salicylic acid (SA), jasmonic acid (JA), and ethylene (ET; Gorman *et al*., 2020; Yuan *et al*., 2019; Zhou *et al*., 2021). SA is particularly effective against piercing-sucking insects and biotrophic pathogens, whereas JA and ET are more effective against chewing insects and necrotrophic pathogens (Moreira and Abdala-Roberts, 2018; Xu *et al*., 2021). Furthermore, maize plants utilize elicitor peptides, such as ZmPep1 and ZmPep3, to regulate their resistance to fungal pathogens and defence against herbivores (Huffaker *et al*., 2013). In addition to direct defence mechanisms, maize plants also release volatile organic compounds in response to herbivores, which act as defence signals to attract herbivore predators in search of prey or hosts (Degenhardt *et al*., 2009; Vaughan *et al*., 2018). Recently, the pathogen-induced unique ent-CPS-dependent diterpenoids dolabralexins and kauralexins were shown to have bioactivity against

Please cite this article as: Liu, C., He, S., Chen, J., Wang, M., Li, Z., Wei, L., Chen, Y., Du, M., Liu, D., Li, C., An, C., Bhadauria, V., Lai, J. and Zhu, W. (2023) A dual-subcellular localized β-glucosidase confers pathogen and insect resistance without a yield penalty in maize. *Plant Biotechnol. J.*, https://doi.org/10.1111/pbi.14242.

pathogens in maize (Christensen *et al.*, 2018; Ding *et al.*, 2019; Fu *et al.*, 2016; Mafu *et al.*, 2018). As a class of the most studied defensive compounds in maize, benzoxazinoids also play an important role in resistance against herbivores and fungal invasion (Ahmad *et al.*, 2011; Balmer *et al.*, 2013; Ye *et al.*, 2019; Zhang *et al.*, 2021). In addition, corn utilizes defence components in the plant cell wall to resist various pests and diseases. For example, lignin, as the second most abundant biopolymer in the cell wall, is important for stem hardness and resistance to pests and diseases (Barros *et al.*, 2015; Bhuiyan *et al.*, 2009; Sun *et al.*, 2018).

The benzoxazine (Bxs) metabolites are a class of compounds that provide insecticidal and disease-resistant properties in maize (Makowska *et al.*, 2015; Zhang *et al.*, 2021). The maize genome encodes a set of enzymes (BX1 to BX9) that are responsible for converting indole-3-glycerol phosphate to 2,4-dihydroxy-7-methoxy-1,4-benzoxazin-3-one glucoside (DIMBOA-Glc). DIMBOA-Glc can be hydroxylated by O-methyltransferase (BX10-BX12) to form 2-hydroxy-4,7-dimethoxy-1,4-benzoxazin-3-one glucoside (HDIMBOA-Glc; Meihls *et al.*, 2013). Both DIMBOA-Glc and HDMBOA-Glc are stored in vacuoles, and can be further hydrolyzed by specific glucosidases during cellular damage or disruption, resulting in the formation of toxic DIMBOA and HDMBOA (Glauser *et al.*, 2011; Zhang *et al.*, 2021). The auxin-regulated protein ZmAuxRP1 was shown to contribute to stalk rot resistance by enhancing the accumulation of DIMBOA-Glc in maize (Ye *et al.*, 2019). In addition, treatment of maize leaves with DIMBOA-Glc and DIMBOA has been shown to decrease the body weight of the first-instar larvae of common maize pests (Zhang *et al.*, 2021).

Lignin is a biopolymer that not only plays roles in growth and development of plants but also is an important physical barrier for plants to resist pathogenic invasion (Barros *et al.*, 2015; Cesarino, 2019; Malinovsky *et al.*, 2014; Sattler and Funnell-Harris, 2013; Vanholme *et al.*, 2010). During pathogenic invasion, the expression levels of lignin biosynthetic genes and lignin accumulation increase significantly (Lee *et al.*, 2019; Wei *et al.*, 2021). In model plant *Arabidopsis thaliana*, knockout mutants of lignin biosynthetic genes phenylalanine ammonia lyase (*PAL*), caffeic acid O-methyltransferase (*COMT*), and cinnamyl alcohol dehydrogenase (*CAD*) showed reduced resistance against various pathogenic bacteria and fungi, including *Pseudomonas syringae*, *Alternaria brassicicola*, *Botrytis cinerea*, and *Blumeria graminis* (Ninkuu *et al.*, 2022; Quentin *et al.*, 2009; Tronchet *et al.*, 2010). Similarly, in crops, suppression of *PAL*, *COMT*, and *CAD* increases the susceptibility of hosts to pathogenic fungi (Bhuiyan *et al.*, 2009; Lee *et al.*, 2019). Moreover, lignin-deposited structure can serve as a physical barrier similar to the Casparian strip to limit the expansion of pathogens in the extracellular matrix and enhance plants' resistance to diseases (Lee *et al.*, 2019).

Glycoside hydrolase family 1 (GH1) β-glucosidases (EC 3.2.1.21), which catalyse the hydrolysis of β-glycosidic bonds in a variety of substrates, are widely distributed in animals, plants, and microorganisms. (Baiya *et al.*, 2018; Ketudat Cairns *et al.*, 2015; Wang *et al.*, 2020). The β-glucosidases are key enzymes in the biosynthesis of the benzoxazinoid compound DIMBOA. The benzoxazinoid compound DIMBOA-Glc is stored in the vacuole, while under pathogens and feeding pests invasion, the DIMBOA-Glc is then converted as the defence compound DIMBOA by β-glucosidases (Glauser *et al.*, 2011; Meihls *et al.*, 2013; Zhang *et al.*, 2021). In addition, β-glucosidases release monolignin from lignin glycoconjugates in the cell wall, and thus increase lignin accumulation (Baiya *et al.*, 2018; Liu *et al.*, 2011; Perkins *et al.*, 2019).

Here, we reported the discovery of a dominant Pythium stalk rot resistance gene *ZmBGLU17* in maize. *ZmBGLU17* was discovered via GWAS for stalk rot resistance, and it encodes a β-glucosidase with a secretory signal peptide, which can not only be secreted into the apoplast but also released into the vacuole, resulting in the accumulation of defence metabolites, including both lignin and DIMBOA in maize. Infection assay showed that this novel glycoside hydrolase with a dual-subcellular localization confers broad-spectrum resistance to both pathogens and herbivorous insects simultaneously without a yield penalty in maize.

Results

GWA study of *Pythium* stalk rot resistance in maize inbred lines

To investigate the resistance of maize to *Pythium aphanidermatum*, Pythium stalk rot was determined by the degree of primary root susceptibility of maize seedlings 24 h after inoculation (h.p.i.) with *P. aphanidermatum* in a maize natural variation population consisting of 189 distinct maize inbred lines (Table S1). This maize population comprises tropical or subtropical inbred lines, temperate lines, and mixed origin (Yang *et al.*, 2011). The severity of root infection was scored on an arbitrary scale from 0 to 4, based on the biomass of *P. aphanidermatum* in the inoculated roots, using at least three biological replicates for each line (Figure 1a). The disease phenotypes were normally distributed (Figure S1a). Using the mix linear model (MLM), GWA analysis identified 43 single nucleotide polymorphisms (SNPs) above the suggestive significance threshold for an association ($p < 1.0 \times 10^{-4}$; Figure 1b; Figure S1b). These significant SNPs corresponded to 16 loci on chromosomes 1, 2, 3, 5, 6 and 8 (Table S2).

ZmBGLU17 is significantly associated with *Pythium* stalk rot resistance

The most significant SNP chr1.S_264854246 ($P < 1.13 \times 10^{-5}$) is located in the 5′-untranslated region (5′-UTR) of a single gene (*AC217401.3*) on chromosome 1. *AC217401.3* is predicted to encode β-glucosidase 17, a member of the glycosyl hydrolase 1 family. We named this gene *ZmBGLU17* according to the previous classification (Gómez-Anduro *et al.*, 2011). The ten SNPs located in the coding region of *ZmBGLU17* form two blocks of linkage disequilibrium (LD; Figure 1c), which distinguish the 189 maize inbred lines into two haplotype groups (Figure 1d). Of these, 131 inbred lines belong to the resistant haplotype (Hap1, with a mean DSS of 1.5), and 26 belong to the susceptible haplotype (Hap2, with a mean DSS of 2.1). Statistically, the lines with Hap1 had a significantly lower DSS than those with Hap2 ($P = 7.0 \times 10^{-3}$). Therefore, we designated Hap1 and Hap2 as the resistant and susceptible alleles of *ZmBGLU17*, respectively (Figure 1e).

The roots of GEMS10 (representing Hap1) grew normally after pathogen infection, and browning at the root tip was almost invisible at the inoculation site. In contrast, in TY4 (representing Hap2), the growth of the radicular root was markedly inhibited, and the root tip was seriously infected with *P. aphanidermatum*, with marked browning at the inoculation site. The infection phenotype of the F_1 plants derived from a cross between GEMS10 and TY4 resembled that of GEMS10 (Figure 2a). Statistical analysis showed that the GEMS10 is more

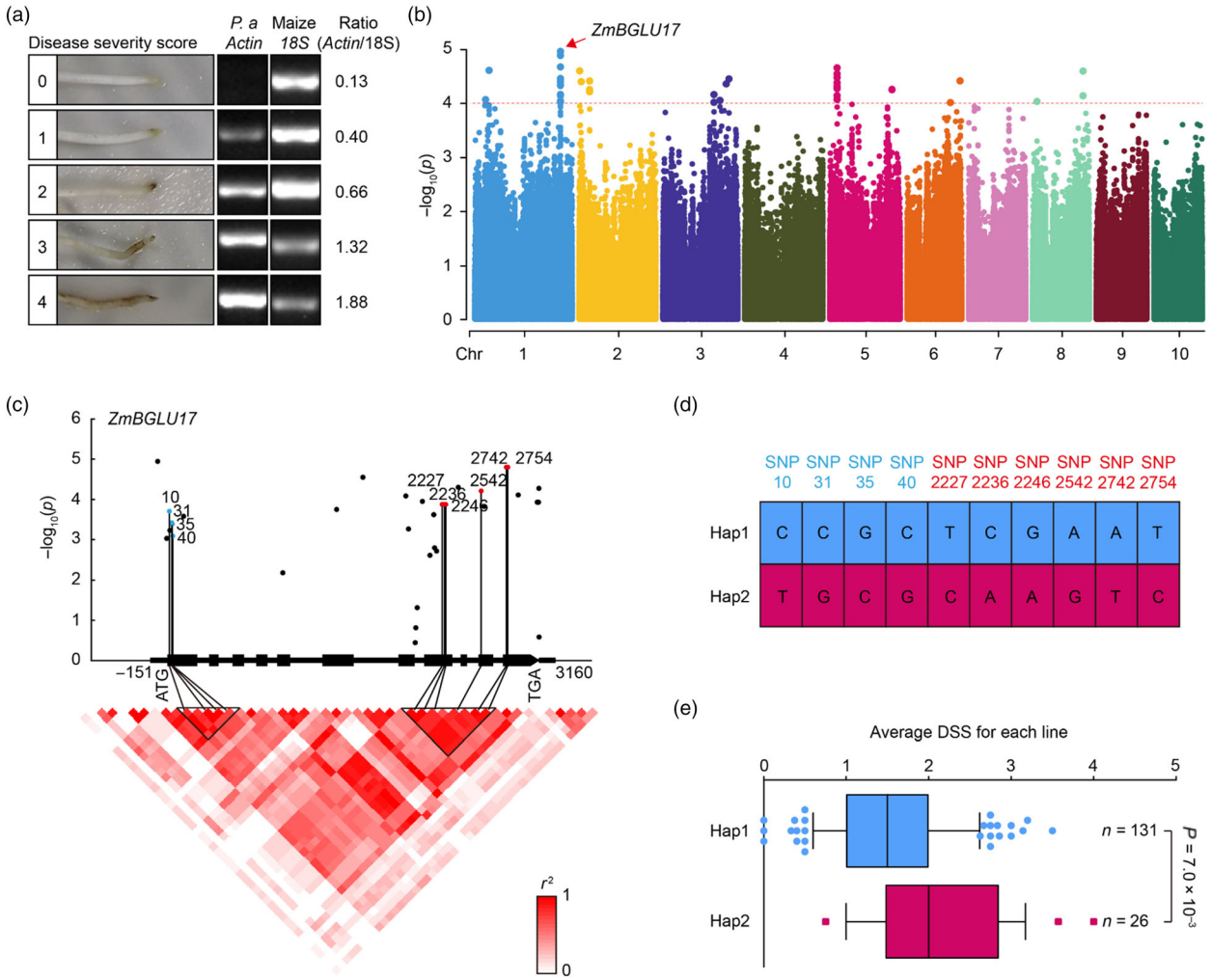

Figure 1 GWAS for *P. aphanidermatum* resistance in maize. (a) According to the invasion of *P. aphanidermatum* on the roots, the disease severity score (DSS) in maize is classified from 0 to 4. (b) Manhattan plot of the GWAS for *Pythium* infection in 189 maize inbred lines. The dashed horizontal line depicts the significance threshold ($P = 1.0 \times 10^{-4}$). (c) *ZmBGLU17*-based association mapping and pairwise LD analysis. Dots represent SNPs. The major SNP in *ZmBGLU17* signal peptide is highlighted in blue and the major SNP in CDS is highlighted in red. The SNPs showing strong LD with the major SNP are formed LD blocks with solid lines and inverted triangles. (d) Haplotypes (Hap) of *ZmBGLU17* among maize inbred lines. (e) Box plot of the average disease severity score distribution of each haplotype group. *n* denotes the number of genotypes belonging to each haplotype group. Statistical significance was determined using a two-tailed Student's *t*-test.

resistant than TY4 ($P = 8.14 \times 10^{-8}$; Figure 2a). Accordingly, the biomass of *P. aphanidermatum* in the root of TY4 is significantly higher than that of GEMS10 ($P = 4.78 \times 10^{-7}$; Figure 2a). Notably, F_1 plants were more resistant to *P. aphanidermatum* infection in comparison to the parents (Figure 2a). In F_2 population, the root tip phenotype of Hap1 (with a mean DSS of 1.47) significantly differed from that of Hap2 (with a mean DSS of 2.2; $P = 1.8 \times 10^{-2}$), while the phenotype of the heterozygote (with a mean DSS of 1.6) was intermediate between the two haplotypes (Figure 2b). This suggested that *ZmBGLU17* is co-segregating with the disease phenotype, which was further validated using whole seedlings for *P. aphanidermatum* infection in the F_2 population (Figure 2c). These findings together indicate that $ZmBGLU17^{GEMS10}$ acts as a positive regulator with additive effects in conferring resistance to *P. aphanidermatum*.

To validate the role of *ZmBGLU17* in maize resistance to Pythium stalk rot disease, we firstly utilized the VIGS gene silencing toolkit to down-regulate the *ZmBGLU17* gene expression in maize and then inoculated the detached leaves with *P. aphanidermatum*. The results showed that the *ZmBGLU17*-silenced plants had significantly longer lesion lengths compared to control plants, suggesting that down-regulation of *ZmBGLU17* in maize increased susceptibility to *P. aphanidermatum* (Figure 2d). Consistently, the roots of *ZmBGLU17* overexpression lines OE1 and OE2 exhibited increased resistance to *P. aphanidermatum* infection in comparison to the control plant (Figure 2e). Moreover, indoor pot experiments showed that the two overexpression lines OE1 and OE2 were more resistant to *P. aphanidermatum* than ND101 at the seedling stage (Figure 2f). Taken together, these results demonstrate that *ZmBGLU17* is one of the underlying resistance genes from the GWA peak.

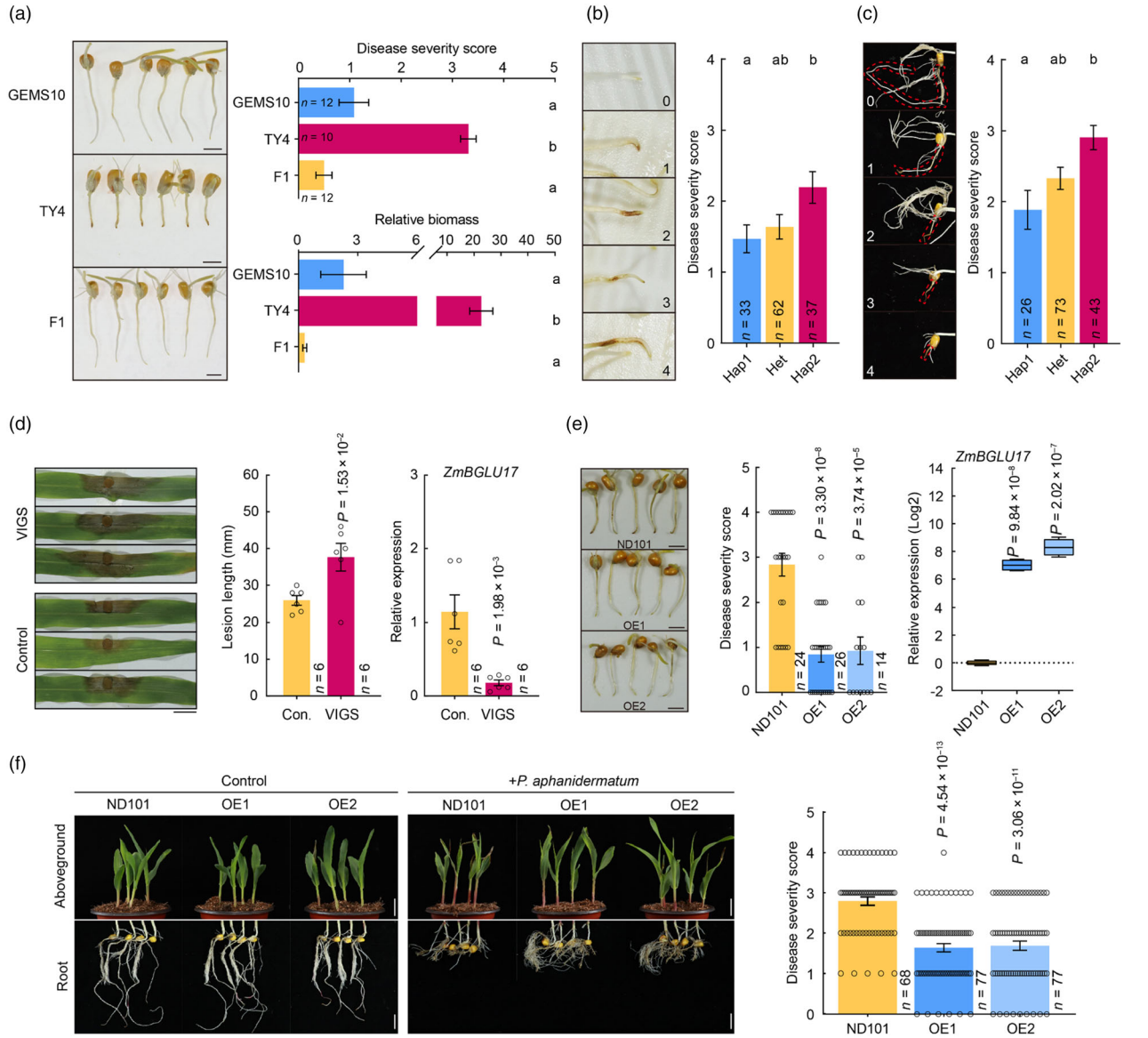

Figure 2 *ZmBGLU17* was significantly associated with Pythium resistance. (a) Representative phenotype (left) and disease severity score (top-right) of Pythium infected roots from GEMS10, TY4 and their crossbred F_1 generation at 24 h.p.i. Scale bars = 10 mm. Lower-right, relative biomass of *P. aphanidermatum* in the radicle root of maize. The *P. aphanidermatum*-specific primers and *Zm18S*-specific primers for relative biomass were determined by qRT-PCR. (b) Phenotypic grading (left) and disease severity score (right) of the roots of the F_2 population inoculated with *P. aphanidermatum* by maize radicle root inoculation. (c) Left, phenotypic grading and disease severity score of the roots from different genotypes of the F_2 population infected with the Pythium-inoculated wheat kernels. *n* denotes the number of plants belonging to each haplotype group. Different letters indicate that significant differences between groups are determined using one-way analysis of variance (ANOVA; $P < 0.05$). (d) Representative phenotype (left) and lesion length (middle) of *P. aphanidermatum* infection at 48 h.p.i. on the second leaf of 14-day-old maize after knockdown of *ZmBGLU17* using VIGS system. The right image represents the relative *ZmBGLU17* mRNA expression levels in leaves from control lines and the VIGS plants at 14 d.p.i. Scale bars = 1 cm. (e) Representative phenotype (left) and disease severity score (middle) of *P. aphanidermatum* infection on the root from the *ZmBGLU17* overexpressing (OE) and ND101 lines. Scale bars = 1 cm. The right image shows the relative expression levels of *ZmBGLU17* in maize materials ND101, OE1, and OE2 determined by RT-qPCR. (f) the left image depicts the phenotype of aboveground and root parts of transgenic maize seedlings grown in pot for 7 days. The middle image shows the representative phenotype of aboveground and root of maize seedlings inoculated with *P. aphanidermatum* at 7 d.p.i. The right image displays the disease severity score statistics with error bars of ± SEM. Scale bars = 2 cm.

ZmBGLU17^{GEMS10} is a positive regulator of *P. aphanidermatum* in maize

There were no significant differences in the expression level of *ZmBGLU17* between the two inbred lines in the absence of pathogen (Figure 3a). However, within 48 h after *P. aphanidermatum* inoculation, the expression of *ZmBGLU17* in GEMS10 gradually increased, while it significantly decreased in TY4 (Figure 3a). As expected, the expression levels of *ZmPR4*, a marker gene involved in plant defence response, were upregulated in both haplotypes after induction, with a stronger response observed in the resistance inbred line GEMS10 (Figure 3b),

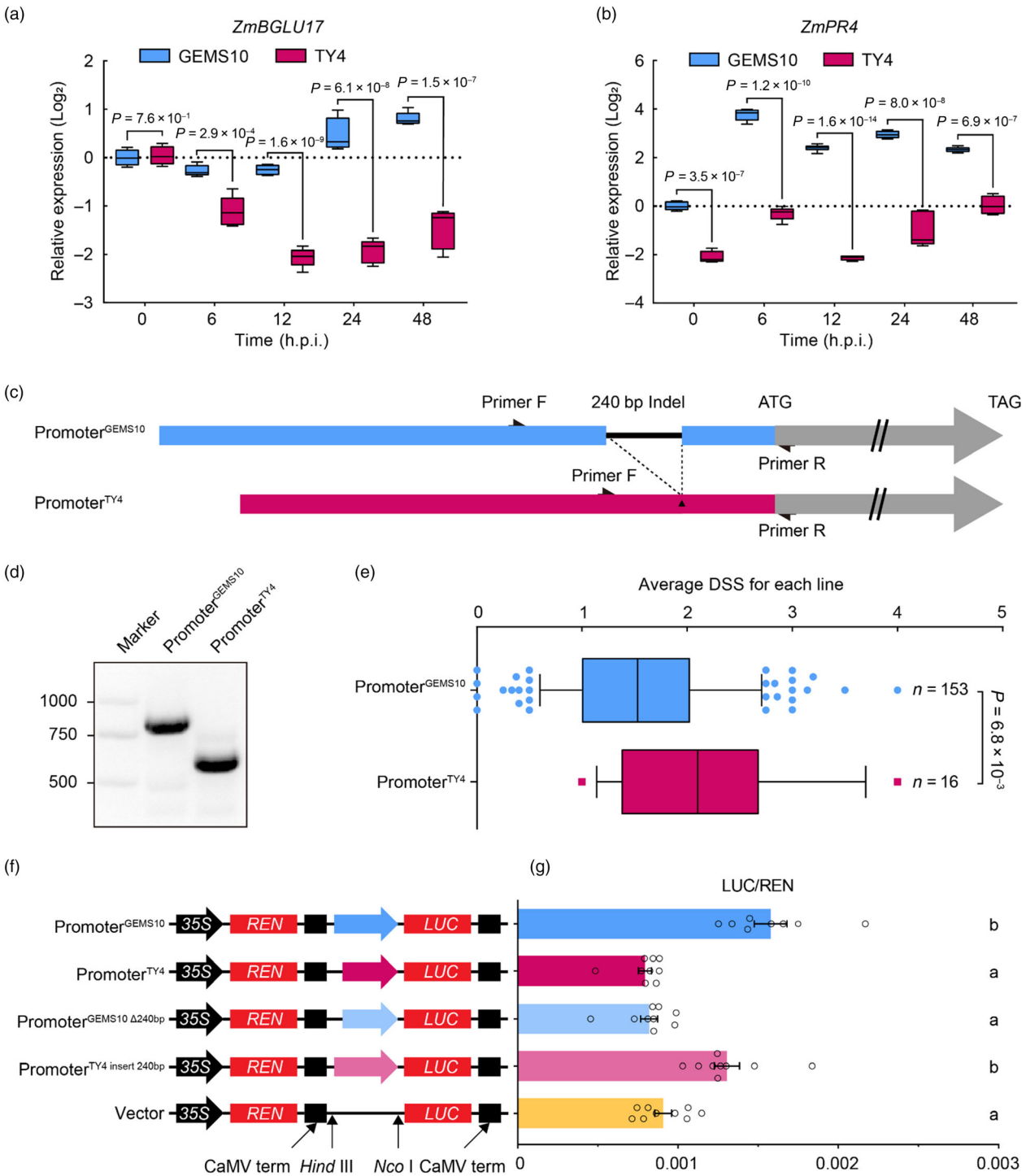

Figure 3 The 240-bp insertion in promoter enhances the transcriptional efficiency of ZmBGLU17^{GEMS10}. (a) and (b) showed the gene expression of *ZmBGLU17* and *ZmPR4* in response to *P. aphanidermatum* infection from GEMS10 and TY4 lines. (c) Schematic diagram of Promoter^{GEMS10} and Promoter^{TY4}. The triangle represents 240-bp insertion. The blue area shows the promoter structure of *ZmBGLU17*^{GEMS10}, and red indicates *ZmBGLU17*^{TY4}. Black arrow indicates a pair of detection primers detecting 240-bp insert. (d) Detection of Promoter^{GEMS10} and Promoter^{TY4} by agarose gel electrophoresis. (e) The average DSS of maize inbred lines between two types of promoter. (f) Schematic diagrams of the difference of *ZmBGLU17* promoters fused with the *LUC* gene. The *Renilla* luciferase (*REN*) gene driven by the cauliflower mosaic virus (CaMV) 35S minimal promoter was used as a control. (g) The activity of the different types of *ZmBGLU17* promoters from GEMS10 and TY4. The Promoter^{GEMS10} and Promoter$^{TY4\ insert\ 240bp}$ were associated with stronger normalized luciferase (LUC) activity than Promoter$^{GEMS10\ \Delta240bp}$ and Promoter^{TY4}. Values are means ± SEM. Different letters indicate significant differences ($P \leq 0.05$) as determined by the Student's two-sided *t*-test.

showing that the two *ZmBGLU17* haplotypes respond differently to Pythium infection at the transcriptional level.

To investigate whether natural variations in the promoter and coding region of *ZmBGLU17* of the two haplotypes alter the gene expression, we sequenced full-length *ZmBGLU17* alleles from GEMS10 and TY4, which identified a 240-bp indel (Indel −286) in promoter region and 24 SNPs in the coding region (Figure 3c,d; Figure S2). We named the promoters of these two haplotypes Promoter^{GEMS10} and Promoter^{TY4}, respectively. Using the 240 bp indel as a genetic marker, 153 inbred lines were classified as Promoter^{GEMS10} and 16 inbred lines were classified as Promoter^{TY4} (Figure 3e). The disease severity score of Promoter^{GEMS10} for *P. aphanidermatum* was 1.6, significantly lower than that of Promoter^{TY4} with a disease severity score of 2.2 ($P = 6.8 \times 10^{-3}$, Figure 3e).

To understand how the 240-bp indel affects the transcriptional efficiency of the ZmBGLU17 promoter, we conducted a transient dual-luciferase expression assay in maize protoplasts that were transformed with Promoter^{GEMS10}, Promoter^{TY4}, Promoter$^{GEMS10\ \Delta 240bp}$, and Promoter$^{TY4\ insert\ 240bp}$ of *ZmBGLU17* (Figure 3f). Overall, Promoter^{GEMS10} from both lines resulted in the higher normalized luciferase activity (LUC) than Promoter^{TY4}. The LUC activity driven by Promoter$^{GEMS10\ \Delta 240bp}$ was significantly reduced, similar to Promoter^{TY4}. In contrast, the LUC activity driven by the Promoter$^{TY4\ insert\ 240bp}$ was significantly increased, almost reaching the level of Promoter^{GEMS10} (Figure 3f,g). These results suggest that the 240-bp indel in the promoter affects the expression of the *ZmBGLU17*.

A SNP near the splice donor site in intron 5 triggers alternative splicing of *ZmBGLU17*^{TY4} with non-functional ZmBGLU17 protein

The *ZmBGLU17* is predicted to have a single transcript according to the MaizeGDB database. We indeed observed a single transcript species with expected size from the resistance allele *ZmBGLU17*^{GEMS10}, but isolated three splice forms of *ZmBGLU17* transcripts, designated as *SF1*^{TY4}, *SF2*^{TY4}, *SF3*^{TY4}, from the susceptible inbred line TY4 (Figure 4a,b). The *SF1*^{TY4} transcript is predicted to encode a full-length ZmBGLU17 protein with 506 amino acids, similar to *ZmBGLU17*^{GEMS10}, whereas the *SF2*^{TY4} transcript encodes a protein that lacks 10 amino acids near the enzyme activity center, resulting in a length of 496 amino acids. The *SF3*^{TY4} transcript is predicted to have a premature stop codon, resulting in a truncated protein of 176 amino acids (Figure 4a,e; Figure S3).

Sequence comparison revealed that the *SF2*^{TY4} transcript is a result of alternative splice donor site usage at exon 4, and the *SF3*^{TY4} transcript is caused by the retention of the fifth intron. We hypothesized that genetic variations at or near the splicing site of intron 5 are responsible for the generation of the two unexpected splicing forms *SF2*^{TY4} and *SF3*^{TY4}. Sanger sequencing of the genomic fragment of *ZmBGLU17*^{TY4} revealed a mutation from 'a' to 't' at the +4 position base of the fifth intron of *ZmBGLU17*^{TY4} (Figure S4). This mutation is noteworthy because a recent study has shown that SNPs near the splice donor site 5′-GT are critical for proper mRNA splicing (Wang *et al.*, 2019). To validate the natural variation at the +4 position of the fifth intron as a crucial determinant for the alternative splicing of *ZmBGLU17*^{TY4}, we introduced a t4a mutation at this site in *ZmBGLU17*^{TY4}. As shown in Figure 4c, RT-PCR revealed predominantly *SF1* transcripts for *ZmBGLU17*^{TY4} with the t4a mutation, albeit with faint *SF3* signal, resembling the transcriptional pattern of *ZmBGLU17*^{GEMS10} in *N. benthamiana*. Similarly, *ZmBGLU17*^{GEMS10} with an a4t mutation primarily yielded *SF3* transcripts, with barely detectable *SF1*, mirroring the transcriptional pattern observed for *ZmBGLU17*^{TY4} (Figure 4c). Although the transcriptional profiles of *ZmBGLU17* in *N. benthamiana* was slightly different from maize, these results confirmed that the natural variation at the +4 position of the fifth intron in *ZmBGLU17* is a pivotal factor driving the alternative splicing of *ZmBGLU17*^{TY4}.

The *in vitro* assay of the β-D-glucosidase activity of ZmBGLU17 showed that SF1^{GEMS10} and SF1^{TY4} has similar level of β-D glycosidase enzymatic activity although they differs in several amino acid residues. However, the other two transcripts in TY4, SF2^{TY4}, and SF1$^{GEMS10\ \Delta 30\ bp}$ lacking 10 amino acid and truncated SF3^{TY4} almost lost the β-D glycosidase enzymatic activity (Figure 4d,e). The relative expression levels of functional transcript *SF1* were significantly lower in TY4 than GEMS10 (Figure 4f), suggesting that there is less functional ZmBGLU17 in the susceptible line TY4. These findings together confirm that only the *SF1* transcript encodes a functional ZmBGLU17 protein with β-D glycosidase enzymatic activity, while other splicing forms due to the a4t polymorphism encode non-functional proteins.

To address whether the a4t polymorphism affects disease resistance in maize, we designed dCAPs markers for the a4t site in the fifth intron and identified four inbred maize lines with a4t variations out of 189 lines tested. Those four inbred lines share the same Promoter^{TY4} type promoter of *ZmBGLU17*. We then attempted to compare the disease resistance phenotype between those four inbred lines with other 11 inbred lines shared with the same TY4-type promoter of *ZmBGLU17*. RT-PCR confirmed that *ZmBGLU17* from the four TY4-type maize inbred lines express three transcripts similar to *ZmBGLU17*^{TY4}, whereas *ZmBGLU17* from all GEMS10-type inbred lines had only one transcript *SF1* (Figure 4g). As expected, the four TY4-type inbred lines are more susceptible to *P. aphanidermatum* infection than the 11 GEMS10-type inbred lines (Figure 4g). Taken together, these results suggest that the SNP near splicing donor site triggers alternative splicing of *ZmBGLU17*^{TY4} and subsequently led to non-functional protein, which accounts for susceptibility of maize to *P. aphanidermatum* infection.

ZmBGLU17 localizes at both apoplast and vacuole and contributes to the accumulation of the defence metabolites lignin and DIMBOA

ZmBGLU17 is predicted to encode a signal peptide, indicating that it is a secreted protein (Figure S5a). As expected, the full-length ZmBGLU17-SF1 proteins from both GEMS10 and TY4 can be detected in the extracellular matrix, despite the four natural variations in amino acids between the signal peptide of proteins encoded by the two alleles (Figure S5b–d). However, the SF2^{TY4}-Flag and SF1$^{GEMS10\ \Delta 30bp}$-Flag lacking 10 aa were not detected in the extracellular matrix (Figure S5e). These results suggest that alternative splicing forms but not variations in the signal peptide sequence explain the functional difference of the two alleles encoded ZmBGLU17 (Figure S5).

To further elucidate the exact subcellular localization of different transcripts of *ZmBGLU17*, we constructed fusion proteins of SF1^{GEMS10}, SF1^{TY4}, SF2^{TY4}, and SF3^{TY4} with mCherry tag for confocal imaging. The results showed that the mCherry fluorescence signals of SF1^{GEMS10} and SF1^{TY4} are detectable in both the cytoplasm and the extracellular space, whereas the mCherry fluorescence signals of SF2^{TY4} and SF3^{TY4} cannot be detected in the extracellular region (Figure 5a). Together with the

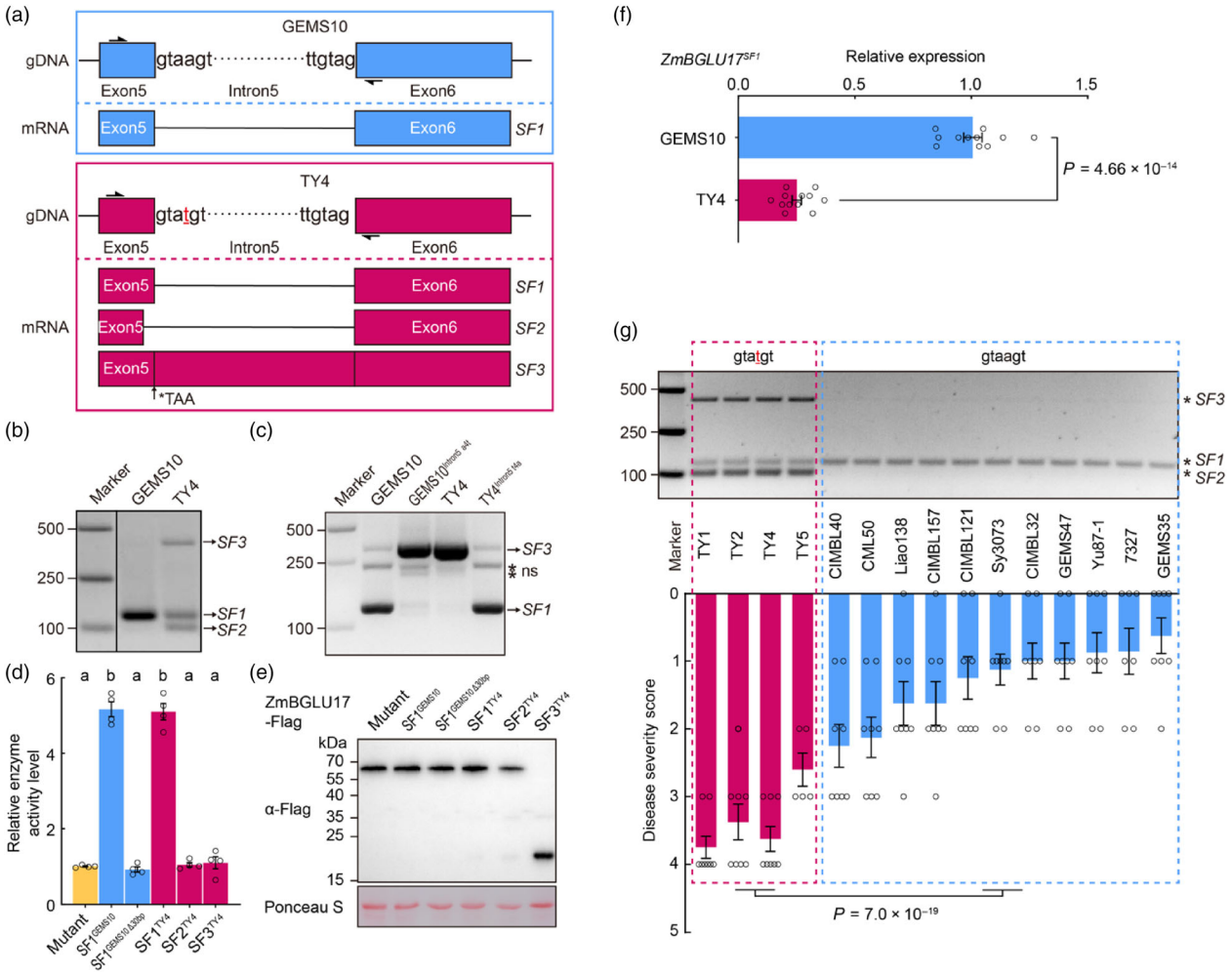

Figure 4 Natural variation of the fifth intron leads to the alternative splicing of *ZmBGLU17*^{TY4}. (a) Gene model for *ZmBGLU17* alternative splicing site. Black arrow indicates a pair of detection primers that detects alternative splicing. (b) RT-PCR validation of the transcription of *ZmBGLU17* in GEMS10 and TY4 maize inbred lines. (c) Detection of alternative splicing of *ZmBGLU17* from GEMS10 and TY4 by transient expression of ZmBGLU17 in *N. benthamiana*. 'ns' indicates nonspecific band. (d) Statistical column chart of relative β-D glucosidase enzymatic activity of ZmBGLU17^{GEMS10} and ZmBGLU17^{TY4} and their mutant proteins. Values are means ± SEM, Different letters indicate significant differences ($P \leq 0.05$) as determined by the one-way ANOVA. (e) Western blot detected the transcript of enzymatically inactive mutants of ZmBGLU17 and their transcripts in GEMS10 and TY4. (f) Detection of expression levels of *ZmBGLU17* transcript SF1 in GEMS10 and TY4 by qRT-PCR. (g) Natural variations at the fifth alternative splicing site of *ZmBGLU17* (upper) and phenotypes of the root inoculation in maize inbred lines (lower).

result from protein fractionation assay (Figure S5), we concluded that ZmBGLU17^{SF1} is an extracellular localized protein. The extracellular β-glucosidases are known to release monolignin from lignin glycoconjugates from the cell wall (Baiya *et al.*, 2014) and thus increase lignin accumulation. We, therefore, measured the lignin content in the stem of the parental materials GEMS10 and TY4. Wiesner test (phloroglucinol/HCl) showed that the resistant parental line GEMS10 tended to have more coniferaldehyde incorporation at the cell wall than the susceptible line TY4. In agreement with this, the lignin content in GEMS10 (164.4 ± 4.3 mg/g) was much higher than that of TY4 (83.2 ± 2.5 mg/g; Figure 5b). Consistently, two independent *ZmBGLU17* overexpression lines *ZmBGLU17*-OE1 (OE1) and *ZmBGLU17*-OE2 (OE2) have more coniferaldehyde incorporation at cell wall, and also more lignin content than the control ND101 line (Figure 5c), suggesting that ZmBGLU17 promotes the lignin accumulation in maize.

Although ZmBGLU17^{SF1} is secreted to the extracellular matrix, we noticed that the ZmBGLU17-cherry signal is also detected at the cytoplasm. Since some glucosidases are predicted to localize at vacuoles, we wonder whether the ZmBGLU17^{SF1} is also secreted into vacuoles. To test this hypothesis, SF1^{GEMS10}, SF1^{TY4}, SF2^{TY4}, SF3^{TY4}, and ZmBGLU17$^{\Delta SP}$ without signal peptide, fused with mCherry tag, were transiently expressed in maize protoplasts, using the maize vacuole membrane protein ZmTPK-GFP as a marker for visualizing the vacuoles (Tang *et al.*, 2020). As shown in Figure 5d, the fluorescent signal of SF1^{GEMS10} and SF1^{TY4} but not ZmBGLU17$^{\Delta SP}$ appears in the maize vacuoles, showing that ZmBGLU17^{SF1} localizes in vacuoles. Moreover, the subcellular localization pattern of SF2^{TY4} and SF3^{TY4} is entirely different from that of ZmBGLU17^{SF1}, with no red fluorescent signals detected within the vacuoles (Figure 5d). Together with *in vitro* assay of the β-D-glucosidase activity (Figure 4d), we concluded that only the *SF1*-encoded ZmBGLU17^{SF1} is functional

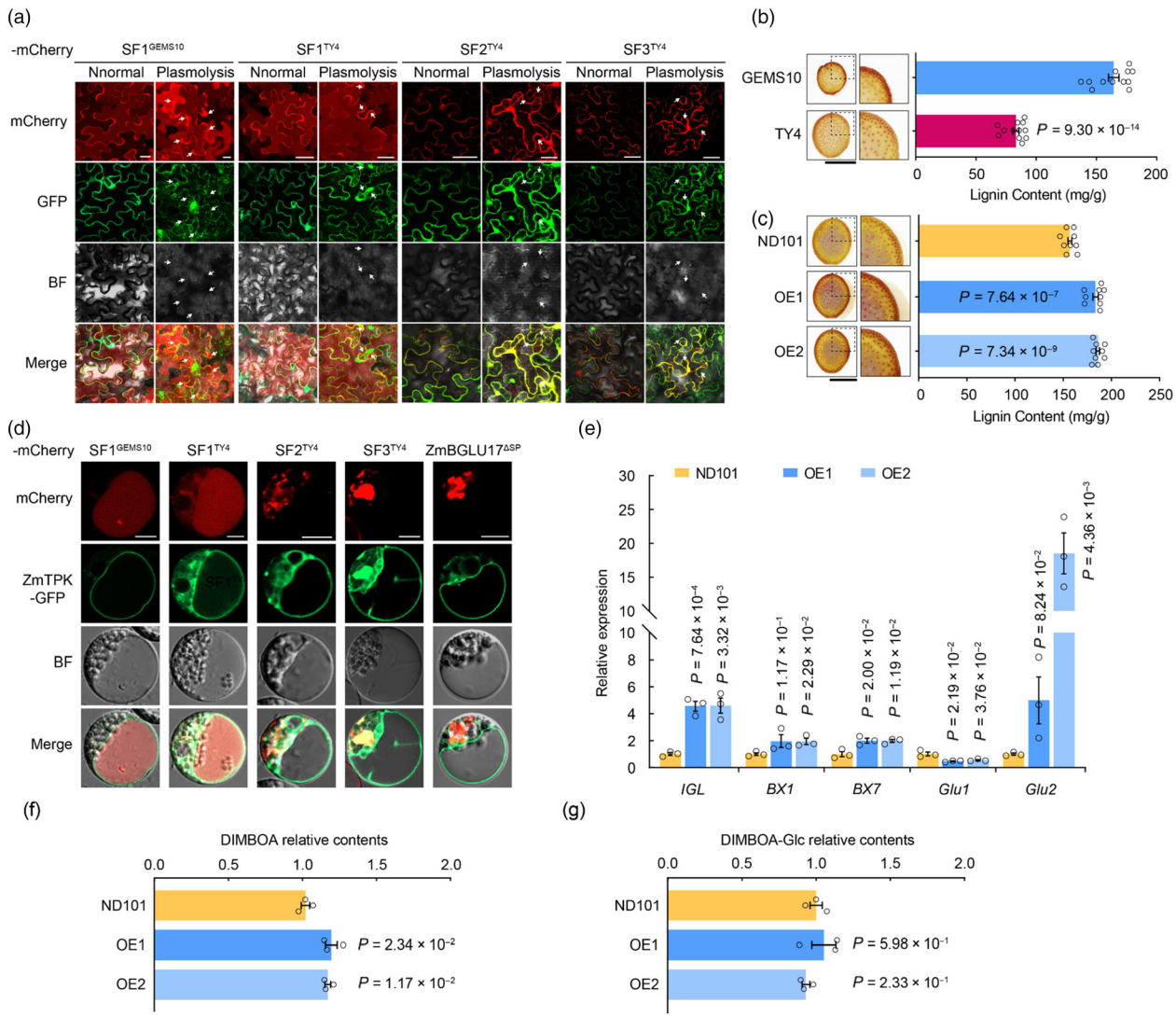

Figure 5 Apoplastic and vacuolar localized ZmBGLU17 contributes to the accumulation of both lignin and DIMBOA in maize. (a) $SF1^{GEMS10}$-mCherry and $SF1^{TY4}$-mCherry were localized in the apoplastic space of *N. benthamiana* cells after plasmolysis. Laser scanning confocal microscopy observed red and green fluorescence in the cytoplasmic lysate cells of *N. benthamiana* cells expressed by GFP together with $SF2^{TY4}$-mCherry and $SF3^{TY4}$-mCherry. The white arrows indicate the periplasmic spaces after *N. benthamiana* cells were plasmolyzed. Scale bar = 20 μm. (b) Left, Phloroglucinol-HCl-stained cross sections of internodes of the GEMS10 and TY4. Right, the lignin content in stems of GEMS10 and TY4. The bar represents 1 cm. Statistical significance was determined using a Student's two-sided *t*-test. (c) Left, Phloroglucinol-HCl-stained cross sections of internodes of the ND101 and ZmBGLU17 overexpress lines. Right, lignin content in stems of ND101, OE1, and OE2. Statistical significance was determined using a Student's two-sided *t*-test. (d) $SF1^{GEMS10}$-mCherry and $SF1^{TY4}$-mCherry localized to the cytoplasm and vacuole in maize protoplasts. Red fluorescence was observed in maize protoplasts transiently expressing $SF1^{GEMS10}$-mCherry, $SF1^{TY4}$-mCherry, $SF2^{TY4}$-mCherry, $SF3^{TY4}$-mCherry, and $ZmBGLU17^{\Delta SP}$-mCherry via confocal microscopy. Green fluorescence indicates the signal of ZmTPK-GFP. Red signals outside the vacuole are autofluorescence from chloroplast. Scale bar = 10 μm. (e) Expression of genes involved in DIMBOA biosynthesis in roots from ND101 and ZmBGLU17-OE lines. (f, g) DIMBOA and DIMBOA-Glc contents from ND101 and ZmBGLU17-OE lines measured by high-performance liquid chromatography analysis.

in maize, while the alternative spliced transcripts *SF2* and *SF3* encoded proteins not only loss the protein functionality, and also localize improperly in maize cells.

Since vascular-localized glucosidases are proposed to catalyse the defensive metabolite DIMBOA-Glc and convert it into functional DIMBOA upon cell rupture caused by pathogen infection or herbivore feeding for defence (Zhang *et al.*, 2021), we wonder whether ZmBGLU17 contributes to DIMBOA metabolism in maize. To test this hypothesis, we quantified the expression of marker genes required for the biosynthesis of DIMBOA in *ZmBGLU17* overexpression lines together with ND101 line. As shown in Figure 5e, two DIMBOA biosynthesis marker genes, *IGL* and *BX1* (Maag *et al.*, 2016), were expressed at a higher level in *ZmBGLU17*-OE lines than the control ND101 line. In addition, the expression levels of DIMBOA biosynthetic pathway-related genes, *BX7*, and *Glu2* (Makowska *et al.*, 2015), were also significantly higher in the OE materials than ND101, although *Glu1* was slightly down-regulated in the OE materials (Figure 5e). In agreement, *ZmBGLU17*-OE lines have significantly higher levels of DIMBOA than ND101, but with a

similar amount of DIMBOA-Glc (Figure 5f,g). These results suggested that ZmBGLU17 contributes to DIMBOA metabolism in vacuoles.

ZmBGLU17 confers resistance to both pathogen and herbivorous insect without yield penalty

Since DIMBOA and lignin are two key secondary metabolites for herbivore insect defence (Diezel *et al.*, 2011; Joo *et al.*, 2021; Zhou *et al.*, 2021), we wonder whether *ZmBGLU17* contributes to herbivore insect resistance. *O. furnacalis* is one of the most damaging herbivore insects in maize production (Guo *et al.*, 2019). We then measured the weights of the insects at three different time points, 48, 72, and 96 h after feeding with *O. furnacalis* in resistant and susceptible lines GEMS10 and TY4. The results showed that the weight of the insects fed with GEMS10 corn leaves was significantly lower than that of the insects fed with TY4 leaves (Figure 6a), suggesting that GEMS10 with $ZmBGLU17^{Hap1}$ is more resistant to *O. furnacalis* than TY4 with $ZmBGLU17^{Hap2}$. Furthermore, the larvae fed with leaves from *ZmBGLU17* overexpression lines were significantly smaller than those fed with leaves from wild-type plants (Figure 6b), showing that increased expression of *ZmBGLU17* enhances maize resistance to herbivorous insects.

To further validate the effectiveness of the resistance gene *ZmBGLU17* against *P. aphanidermatum* infection in the lab condition, we inoculated maize materials overexpressing *ZmBGLU17* with *P. aphanidermatum* for disease assay in field. The results showed that *ZmBGLU17* overexpression lines OE1 and OE2 have significantly lesser severe stalk rot disease phenotype than the control line ND101 (Figure 6c), suggesting that overexpression of *ZmBGLU17* has the potential to enhance maize resistance to Pythium stalk rot caused by *P. aphanidermatum* in field.

Finally, field experiment showed that there are no significant difference in the number of rows per ear and the grain weight per ear between corns with the two alleles of *ZmBGLU17*, although corns with $ZmBGLU17^{GEMS10}$ allele had relatively lighter hundred kernel weight than corns with $ZmBGLU17^{TY4}$ allele, most likely due to other genes rather than *ZmBGLU17* (Figure S6). In agreement with this, *ZmBGLU17* overexpression lines had normal growth in field with similar kernel size and yield as ND101 and vector lines (Figure 6d–f), suggesting that *ZmBGLU17* confers resistance to both pathogen and herbivorous insect without a yield penalty (Figure 7).

Discussion

Maize stalk rot is a soil-borne disease that causes substantial yield loss and quality reduction of maize worldwide (Wang *et al.*, 2017). *P. aphanidermatum* is one of the important pathogens causing stalk rot in maize, but there is limited research on disease resistance genes against Pythium stalk rot in maize (Song *et al.*, 2015; Yang *et al.*, 2002). Despite the popularity of the GWA study in discovering disease resistance genes in maize, there are few reports on resistance genes against Pythium stalk rot. Here, we demonstrated that the *ZmBGLU17* allelic variant confers broad-spectrum resistance against both stalk rot and *O. furnacalis* in maize through the GWA study. A 240-bp indel mutation in the promoter increased the expression level of *ZmBGLU17*, while natural variation at the splicing site of the fifth intron resulted in reduced functional transcripts of *ZmBGLU17*. *ZmBGLU17* exhibited dual localization to the extracellular matrix and vacuoles. Overexpression of *ZmBGLU17* significantly increased the accumulation of lignin and DIMBOA content in maize, thereby enhancing resistance against *P. aphanidermatum* and *O. furnacalis* without a yield penalty.

β-Glucosidase (EC 3.2.1.21) is a cellulase enzyme that catalyses the hydrolysis of non-reducing β-D-glycosidic bonds at the terminal end of sugar-containing compounds, releasing β-D-glucose (Ketudat Cairns and Esen, 2010). Currently, the localization of β-glucosidase primarily relies on the prediction from the CAZy database (http://afmb.cnrs-mrs.fr/CAZY/) and TAIR (http://www.arabidopsis.org/info/genefamily/GlycosideHydrolase.html; Gómez-Anduro *et al.*, 2011; Minic and Jouanin, 2006). There have been limited reports on the experimental determination of subcellular localization of specific glucosidases. In this study, through a series of biochemical experiments and confocal microscopy observations, we demonstrated that the maize β-glucosidase ZmBGLU17 enzyme localizes in both the extracellular matrix and vacuoles, despite ZmBGLU17 being predicted as a vacuole localized protein (Gómez-Anduro *et al.*, 2011). Therefore, experimentally validating the precise subcellular localization of β-glucosidases, besides the prediction from the CAZy database, will be beneficial for better understanding the biological function of those enzymes.

GH1, the largest family of plant glycoside hydrolases, plays a crucial role in plant cell wall formation, activation of plant hormones, and response to biotic and abiotic stresses (Chen *et al.*, 2019; Kong *et al.*, 2019; Ren *et al.*, 2020; Wang *et al.*, 2020; Zagrobelny *et al.*, 2008). Firstly, β-glucosidases can maintain the secondary structure of the cell wall by degrading oligosaccharides in the cell wall and releasing lignin monomers (Ren *et al.*, 2020). For instance, Os4BGlu14, Os4BGlu16, and Os4BGlu18 are considered to be rice monolignol β-glucosidases capable of hydrolyzing monolignol glucosides such as coniferin and syringin (Baiya *et al.*, 2014, 2018). Moreover, the β-glucosidase family plays a significant role in plant defence against environmental stress, by hydrolyzing inert glucosides to release toxic compounds for resisting herbivores and pathogenic fungi (Ketudat Cairns and Esen, 2010). Normally, the benzoxazinoid compound DIMBOA-Glc is typically stored in vacuoles. When plant cells are damaged by herbivores, the DIMBOA-Glc in the vacuoles can be released for defence through the action of specific β-glucosidases, such as Glu1 and Glu2, resulting in the release of the toxic compound DIMBOA (Tzin *et al.*, 2015; Zhang *et al.*, 2021). Although β-glucosidases play crucial roles in lignin synthesis and DIMBOA metabolism, whether individual β-glucosidase is involved in regulating both lignin and DIMBOA metabolism simultaneously is not yet reported. We found that *ZmBGLU17* overexpression lines exhibited higher levels of DIMBOA and lignin content compared to the control, suggesting that ZmBGLU17 is involved in the metabolic regulation of both compounds, which most likely is attributed to the feature of dual localization of ZmBGLU17 in extracellular matrix and vacuoles. Finally, we observed that the relative enzyme activity of ZmBGLU17 was much lower than that of the classical DIMBOA-Glc hydrolyzing enzymes ZmGlu1 and ZmGlu2 (Figure S7). Considering that excessive accumulation of DIMBOA has a negative effect on plant growth (Butrón *et al.*, 2010), we hypothesize that the low enzymatic activity of ZmBGLU17 allows for fine-tuning of the basal levels of DIMBOA for pest resistance with minimal effect on plant growth.

Genes generate different splice isoforms through alternative splicing to regulate expression and function, a phenomenon that

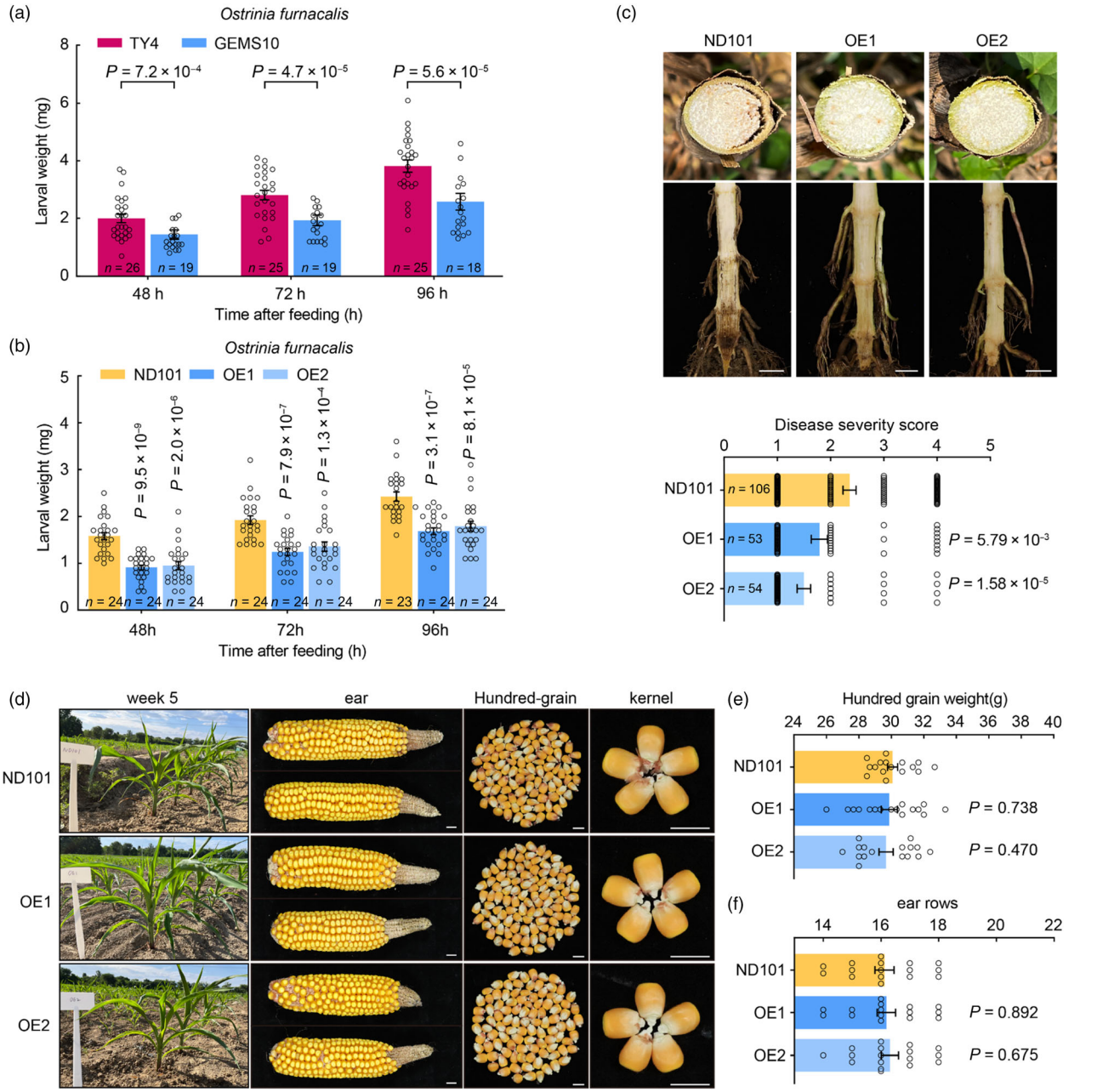

Figure 6 *ZmBGLU17* confers *P. aphanidermatum* and *Ostrinia furnacalis* resistance without a yield penalty. (a) Larval weight after feeding with GEMS10 and TY4 maize leaves (corn V6 stage leaves) at 48, 72, and 96 h. Error bars, ± SEM. (b) Larval weight after feeding with the V6 stage leaf from ND101 and two independent *ZmBGLU17* overexpression lines after 48, 72, and 96 h. Error bars, ± SEM. (c) The phenotype grading (upper) and disease severity score (lower) of Pythium stalk rot of ND101, OE1, and OE2 in field. Error bars, ± SEM. Scale bars = 2 cm. (d) *ZmBGLU17* overexpression transgenic maize materials grown in the field for 5 weeks (left). The ear, hundred-grain, and grain morphology of *ZmBGLU17* overexpression transgenic maize seeds are unaffected (right). Scale bar = 1 cm. The statistical column chart of the hundred kernel weights (e) and the ear rows (f) of *ZmBGLU17* overexpression transgenic maize materials. The hollow black circles represent each data point. Values are means ± SEM, and the significance is estimated by the one-way ANOVA.

is widely present in various biological activities (Filichkin *et al.*, 2015; Guo *et al.*, 2022; Laloum *et al.*, 2018; Lam *et al.*, 2022; Li *et al.*, 2016; Mandadi *et al.*, 2023; Salz, 2011; Xu *et al.*, 2005). It is well known that the splicing site GT-AG motif is crucial for the recognition of mRNA splicing by the spliceosome (Ohno *et al.*, 2018), and natural variations of GT-AG motif are found to be an important genetic basis for plants to adapt to environmental changes. For example, in different ecotypes of *Arabidopsis*, the functional differences of the flowering gene *FLM* depend on the natural variations in the spliceosome recognition sequence GT-AG, leading to the accumulation of non-functional FLM transcripts and consequently affecting the flowering time (Dent *et al.*, 2021; Hanemian *et al.*, 2020). Besides the classical GT-AG site, the nucleotides immediately after the donor site GT, particularly the following four bases, is also crucial for intron processing in mRNA, by affecting the binding affinity between

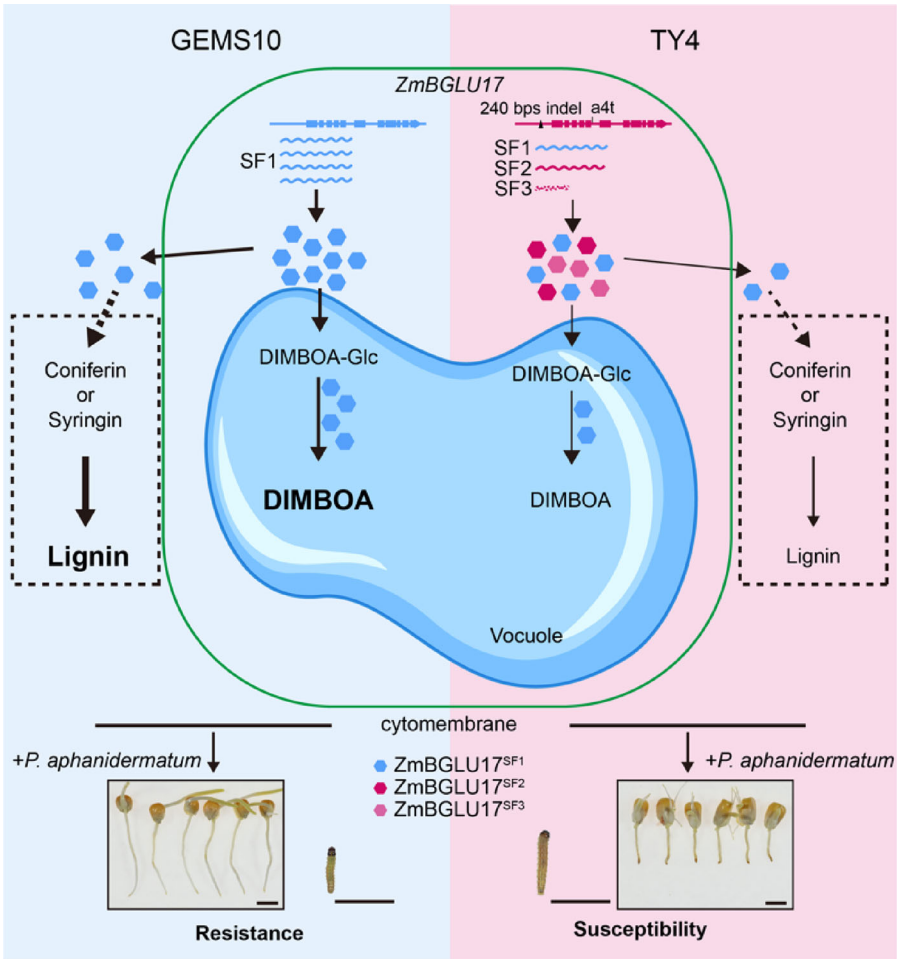

Figure 7 The model of enhanced maize resistance against pests and diseases mediated by *ZmBGLU17* through fine-tuning of lignin accumulation and DIMBOA synthesis. In the susceptible inbred line TY4, *ZmBGLU17* carries a 240 bp indel within its promoter region. This indel significantly influences the expression level of *ZmBGLU17*. Furthermore, a natural variation occurring at the +4 position of 5′ splice site of the fifth intron leads to an alternative splicing event, resulting in the reduction of the functional transcript SF1. This alteration influences the synthesis of the bioactive compound DIMBOA and the accumulation of lignin. By comparison, in the resistant inbred line GEMS10, *ZmBGLU17* responds to pathogen invasion and produces only one functional transcript. ZmBGLU17 fine-tuning of DIMBOA synthesis and lignin accumulation, effectively enhancing the natural resistance to *P. aphanidermatum* and *O. furnacalis* in maize without a yield penalty.

the spliceosome and the intron sequences (Kondo *et al*., 2015). In agreement with this, mutating the nucleotides near the 5′ splice site of *AtFtsZ1* gene in *Arabidopsis* can activate nearby cryptic splice sites, leading to alternative splicing events (Cheng *et al*., 2023). In our study, through forward genetic analysis, we discovered that a natural polymorphism at the +4 position of the 5′ splice site of the fifth intron of *ZmBGLU17*, where an A to T change occurred, leads to the generation of different splice variants, resulting in decrease amount of functional transcript. We thus demonstrated the first example of natural variation of nucleotides near the 5′ splice site affecting mRNA alternative splicing with phenotypic effect. It will be of interest to learn whether this type of polymorphism is widely present in genomes of plants and animals with adaptation significance.

In addition, since the gene with the mutation at nucleotides near the 5′ splice site still encodes a low amount of functional transcripts (Cheng *et al*., 2023), we propose a potential approach to manipulate gene expression by precisely modifying the bases near the splicing site using gene editing tools, which allows to generate knock-down alleles of lethal genes in plants. For instance, a recent finding found that a specific allele of the lethal gene *RBL1* (*RESISTANCE TO BLAST 1*) in rice contributes to a broad-spectrum disease resistance without obvious yield penalty, partially through tuning down the mRNA level of *RBL1* (Sha *et al*., 2023). Alternatively, it will be of interest to generate *RBL1* knock-down alleles through editing the nucleotides near the GT-AG site, and screen new *RBL1* variants with balanced defence and growth.

In conclusion, we identified a dual localized β-glucosidase ZmBGLU17 that contributes to both oomycete pathogen and insect resistance without yield penalty in maize, by enhancing lignin accumulation and DIMBOA synthesis simultaneously. In addition, the identification of the novel natural variation of the 5′ splice site as the causal polymorphism of *ZmBGLU17* in regulating alternative splicing sheds light on the future study of natural variation in plants, and also its application in the generation of transgene-free knock-down allele of lethal genes in plants.

Materials and methods

Maize lines and plant growth conditions

Maize inbred lines were obtained from National Maize Improvement Centre of China (NMICC), China Agricultural University (Beijing, China) and maize genetically modified material were provided by germplasm collections in the National Maize Improvement Center Located at China Agricultural University (Beijing, China). All seeds were germinated at 25 °C in the dark for 3 days in a shallow dish covered by water-soaked blotting paper. Seeds with consistent germination were selected for subsequent experiments. *N. benthamiana* plants were grown in pots in growth chambers under 16 h light at 24 °C/8 h dart at 22 °C with 60% humidity. Soil obtained from Pindstrup Mosebrug A/S was used.

Phenotyping of maize resistance to *Pythium* stalk rot at seedling stage and GWA study

Phenotyping of maize resistance to *Pythium* stalk rot was performed in an association-mapping panel composed of 189 maize inbred lines, which are publicly available at Maizego. For each line, five seeds were placed in a shallow dish (31.5 × 23.5 × 6 cm) and inoculated with *P. aphanidermatum* for 24 h. The infection of *P. aphanidermatum* on the primary roots of corn seedlings was divided into five disease levels. We used the 'ggplot2' package in R to create a histogram displaying the frequency distribution of disease indexes. The GWA study was performed in TASSEL v.5.0 software using high-quality data for the 854 290 SNPs with a minor allele frequency (MAF) ≥0.05. For each inbred line, the average disease severity index was calculated as the final disease severity index. The population structure of 189 inbred lines was re-evaluated. The LD between each pair of SNPs was computed using TASSEL v5.0 (Bradbury *et al*., 2007). The MLM approach controlling population structure was used, and the compromised significance threshold for the GWA study was set as $p < 1.0 \times 10^{-4}$ based on the Bonferroni-adjusted correction of multiple testing.

Extraction and transformation of maize protoplasts

A modified method was used for protoplast isolation and transformation (Yang *et al*., 2013). Briefly, leaf strips from 1-week-old maize seedlings with 1 mm leaf sections were digested in an enzyme solution [20 mM MES (pH 5.7), 1.5% cellulase RS, 0.4% macerozyme R10, 0.5 M mannitol, 20 mM KCl, 10 mM $CaCl_2$, 5 mM β-mercaptoethanol, and 0.1% BSA] for 3 h to release protoplasts. After washing the protoplasts with W5 buffer [2 mM MES (pH 5.7), 154 mM NaCl, 125 mM $CaCl_2$, and 5 mM KCl], they were suspended in MMG solution [0.8 M mannitol, 4 mM MES (pH 5.7), and 15 mM $MgCl_2$] at a density of 5×10^5/mL for transformation. For each 2 mL protoplast, 150 μg of selected plasmid was used for the transformation using PEG solution (40% PEG 4000, 0.2 M mannitol, and 100 mM $CaCl_2$). The transformed protoplasts were incubated with a 10 mL of W5 buffer in the dark for 18 h. The collected protoplasts were used for the next experiment.

Promoter activity assay

For promoter activation assay, the different lengths of the *ZmBGLU17* promoter from GEMS10 and TY4 were cloned: the Promoter^{GEMS10} was 1920 bp, and promoter^{TY4} was 1666 bp upstream of the *ZmBGLU17* start codon; the Promoter^{GEMS10} $^{\Delta 240bp}$ was 1680 bp of the Promoter ^{GEMS10} with a 240 bp deletion upstream of the *ZmBGLU17* start codon; the Promoter^{TY4} insert 240 bp was 1906 bp of the Promoter^{TY4} with a 240-bp insertion from GEMS10 upstream of the *ZmBGLU17* start codon. These promoter segments were modified by introducing a *Hind*III site at the 5′ end and a *Nco*I site at the 3′ end of the sequence, allowing these promoters to be cloned as transcriptional fusions with the *LUC* gene in the pGreenII 0800-LUC vector (The vector is provided by Professor Mingliang Xu, China Agricultural University). The *Renilla* luciferase (*REN*) gene driven by the CaMV 35S minimal promoter was used as an internal reference. The transformed maize protoplasts were incubated at 25 °C for 18 h. The protoplasts were fully lysed in 100 μL of lysis buffer (Promega, E1910) and assayed using the Dual-luciferase Reporter Assay System (Promega, E1910), following the instructions provided with the kit. The ratio of LUC and REN enzyme activities was used to define normalized promoter activity. Each construct was performed with three technical replicates and three biological replicates.

Subcellular localization of ZmBGLU17

The coding sequences of *ZmBGLU17* were amplified from the B73 inbred line and ligated into the pCambia 1300-mCherry vector. The pCambia 1300-GFP was used as an empty vector. These constructs were transformed into *Agrobacterium* strain GV3101 and agro-infiltrated into *N. benthamiana* leaves. The plants with agro-infiltrated leaves were allowed to grow at 25 °C for 2 days under low light conditions. To detect extracellular localization of ZmBGLU17, we co-transiently expressed ZmBGLU17-mCherry and GFP in *N. benthamiana* leaves, using pCambia 1300-GFP as controls. Prior to observation using confocal microscopy, a sterile 0.8 M NaCl solution was injected into the transiently expressed *N. benthamiana* leaves using a needleless syringe. This induced the separation of the plasma membrane from the cell wall in tobacco leaf cells. Using a confocal scanning laser microscope (Zeiss LSM880) with standard filter sets, the GFP and mCherry signals in the lower epidermal cells were detected, photographed, and saved.

Extraction of intracellular fluids from *N. benthamiana* leaves

We used the method described in our previous study (Chen *et al*., 2021) to extract the intercellular fluid from *N. benthamiana* leaves. A syringe was used to Inject 0.1 M sodium phosphate buffer solution (pH 6.5) into the *N. benthamiana* leaves that have been infiltrated and expressed by Agrobacterium for 2 days to infiltrate fully. After gently drying the surface of the leaf, the leaf material was carefully attached to the outer wall of the 20 mL syringe and secured with parafilm to prevent damage to the leaf. The syringe was then inserted into a 50-mL centrifuge tube and centrifuged at 300 g, 4 °C for 15 min. Following centrifugation, the supernatant was collected in a 1.5-mL centrifuge tube and mixed with trichloroacetic acid at a volume ratio of 1 : 5. The mixture was placed on ice overnight to allow precipitation. Subsequently, centrifugation was performed at 20 000 *g*, 4 °C for 15 min, the supernatant was discarded, and the precipitate was washed twice with 1 mL of acetone. After the washes, the remaining acetone was volatilized by treating the sample with a metal bath at 80 °C for 20 min. Then, 50 μL of SDS-loading buffer (8 M urea, 2% SDS, 20% glycerol, 100 mM Tris–HCl pH6.8, 0.004% bromophenol blue) supplemented with 10 mM DTT was added, and the sample was further processed at 80 °C for 5 min.

Ten leaf disks (6 mm in diameter) from infiltrated leaves were ground with 200 μL of loading buffer and used as the control for immunoblotting with anti-Flag (A8592; Sigma-Aldrich).

Protein extraction and immunoblotting

N. benthamiana leaves were harvested at 48 h after agro-infiltration. Four discs (8 mm in diameter) were punched out from the leaves using a hole punch and placed into 1.5 mL centrifuge tubes along with grinding beads. The samples were quick-frozen in liquid nitrogen and ground in an automatic sample rapid grinder (JXFSTPRP-24 L, Shanghai Jingxin Industrial Development co., Ltd.) at 45 Hz for a total of 1 min, with 5-s pauses at 30-s intervals. Next, 200 μL of SDS-loading buffer (8 M urea, 2% SDS, 20% glycerol, 100 mM Tris–HCl pH 6.8, 0.004% bromophenol blue) supplemented with 10 mM DTT was added to each tube, and the samples were denatured at 95 °C. Equal amounts of protein were separated on 10% SDS-PAGE gel and transferred onto a PVDF membrane. After blocking with 5% skim milk, the membrane was incubated overnight at 4 °C with anti-Flag (A8592; Sigma-Aldrich). The membrane was then washed with 1× TBST for 5 min for three times before signal detection. To quantify the protein, the rubisco protein large subunit was stained with Ponceau S and used as a loading control.

RNA extraction and qRT-PCR

Total RNA was extracted using RNA isolater Total RNA Extraction Reagent (Vazyme Biotech Co., Ltd) according to the manufacturer's protocols. cDNA was conducted with a HiScript III 1st Strand cDNA Synthesis Kit (Vazyme Biotech Co., Ltd). qRT-PCR was performed with a ChamQ Universal SYBR qPCR Master Mix (Vazyme Biotech Co., Ltd) in QuantStudio 6 Flex Real-Time PCR System (Thermo Fisher Scientific). The qRT-PCR data was normalized using the *Zm18S* or *ZmActin* gene as internal controls. The relative gene expression was calculated using the $2^{-\Delta\Delta Ct}$ method (Livak and Schmittgen, 2001). The qPCR primer sequences are listed in Table S3.

Pythium aphanidermatum inoculation

Three-day-old maize seedlings were inoculated with *P. aphanidermatum* and incubated for 24 h. The corn seedlings were placed in a shallow dish with the primary root positioned on the same plane. A 1 cm wide filter paper strip was fully soaked in the *P. aphanidermatum* solution and gently pressed onto the root tips. The seedlings were then cultivated at 25 °C in a humid and light-proof environment. The primary root phenotype was recorded for maize that underwent pathogen inoculation from 0 h after inoculation (hai) to 24. Based on the severity of *P. aphanidermatum* infection on the primary roots, different disease grades were assigned. For inoculation, the *P. aphanidermatum* strain was initially grown on a 10% V8 juice medium at 25 °C for 3 days. Twelve plugs with a diameter of 6 mm were taken from the periphery of the 5-day-old culture and placed into a conical flask containing 200 mL of 10% V8 liquid medium (with 0.2% agar). The flask was then incubated at 25 °C and 180 rpm for 3 days. Subsequently, the hyphae were mechanically crushed and used as an inoculum.

Two hundred gram of wheat grains were placed into a sterilization bag and 100 mL of water was added. The bag was sterilized at 121 °C for 30 min and allowed to cool naturally to room temperature. Next, 12 plugs of *P. aphanidermatum* with a diameter of 6 mm were inoculated and cultured at 25 °C for 7 days to obtain a solid inoculum. The solid inoculum was then mixed with sterile soil at a ratio of 1 : 3 (v : v) and distributed into plastic pots with a diameter of 10 cm. Corn seeds, germinated for 2 days, were planted in the fungal soil mixture and covered with a layer of sterile soil. After growing for 7 days under the conditions of 16 h of light at 24 °C/8 h of darkness at 22 °C with 60% humidity, the entire maize seedlings were carefully dissected, and the root phenotypes were counted after cleaning.

The maize kernels were sterilized, inoculated with *P. aphanidermatum*, and then cultured in the dark at 25 °C for 15 days. Artificial inoculation was performed following a method described by Ye *et al*. (2019) during the silking stage of maize at the experimental station of China Agricultural University (Shangzhuang, Beijing). Disease severity was assessed according to the previously published protocols (Yang *et al*., 2010).

Ostrinia furnacalis feeding bioassay

The newly hatched larvae of *O. furnacalis* were reared on artificial diets until the second instar. After a 1-day starvation treatment, the larvae were fed with the maize V6 stage whorl leaves. The maize whorl leaves were washed with sterile water, cut into 1 cm width, and placed in sterile petri dishes, with 10 larvae in each dish. After 48, 72, and 96 h of feeding on maize whorl leaves, the weight of all larvae was recorded, and the experiment was repeated three times.

Enzyme activity assays

β-glycosidase activity was measured using the surrogate substrate 4-Methylumbelliferyl-β-D -glucopyranoside (4-MUG) in a microtiter plate assay (Fia *et al*., 2005). A 200 μM substrate standard solution of 4-MUG (Sigma-Aldrich, M3633) was prepared by dissolving it in DMSO and diluting it with sterile deionized water. Similarly, a 10 μM 4-Methylumbelliferone (4-MU, Sigma-Aldrich, M1381) standard solution was prepared using the same method. Additionally, a 50 mM acetic acid buffer solution at pH5.5 was also prepared. The enzyme solution (100 μL) was incubated with 25 μL of 50 mM acetic acid buffer, 25 μL of a 10 mM 4-MU standard solution, and 25 μL of a 200 μM 4-MUG standard solution at 37 °C for 2 h. The reaction was terminated by adding 20 μL of 1 M NaOH. The fluorescence values were measured at an excitation wavelength of 350 nm and an emission wavelength of 450 nm, and they were labelled as *A*, *B*, and *C*, respectively. Similarly, 100 μL of 50 mM acetic acid buffer was incubated with 25 μL of 50 mM acetic acid buffer, 25 μL of a 10 mM 4-MU standard solution, and 25 μL of 200 μM 4-MUG standard solution. The fluorescence values were measured under the same conditions and labelled as *D*, *E*, and *F*, respectively. The relative enzyme activity was calculated using the following formula:

$$\{[(E-D)\times(C-A)/(B-A)]-(F-D)\}_{Treatment} / \{[(E-D)\times(C-A)/(B-A)]-(F-D)\}_{Control}$$

ZmBGLU17-CMV VIGS in maize

Constructs pCMV101, pCMV301 and pCMV201 were provided by Dr. Zhou at China Agricultural University, Beijing. For VIGS assessment, a 234-bp *ZmPDS* fragment utilized previously by Ding *et al*. (2006) was selected for insertion into the CMV VIGS vector. A 229 bp cDNA fragment corresponding to *ZmBGLU17* was selected after analysis to minimize off-target silencing using primer analysis software (https://www.zhaolab.org/pssRNAit/). The cDNA fragment was amplified using appropriate primer sequences (Table S3), and cloned into pCMV201-2b$_{N81}$ by restriction using enzymes *Kpn*I and *Xba*I followed by ligation. The constructed pCMV101,

pCMV301, and pCMV201 and their derivatives were introduced into *Agrobacterium tumefaciens* strain C58C1. *A. tumefaciens* cultures containing pCMV101, pCMV301, and pCMV201 were prepared using the methods described above and infiltrated leaves of *N. benthamiana* inoculated with barley streak mosaic virus (Yuan *et al*., 2011). At 4 days post-infiltration, the infiltrated leaves of *N. benthamiana* were harvested, grind in 0.1 M phosphate buffer (pH 7.0) and centrifuged at 3000 ***g*** for 3 min at 4 °C. Maize seeds were inoculated with the supernatant containing the crude virus extract by the vascular puncture inoculation method (Wang *et al*., 2016), before germinating at 25 °C in the dark for 2 days. The germinated seeds were planted in pots with a diameter of 10 cm, and were cultured in the dark at 18 °C for 8 h and light at 20 °C for 16 h. After 7 days, pick out the plants with mosaic phenotype and continue to cultivate to the V4 stage for use.

Quantification of lignin

Total lignin in maize stems was determined using the phloroglucinol-HCl (Wiesner) reaction (Veronico *et al*., 2018). The Wiesner reagent consists of 1% phloroglucinol (Macklin, P815665) in 99.5% ethanol mixed with 12 M HCl (1 : 1, v : v). Quantification of lignin was performed using a lignin content assay kit (Solarbio, BC4205) based on the acetyl bromide (AcBr) method following the instructions provided in the manual.

Quantification of DIMBOA and DIMBOA-Glc

The maize seeding roots from differentially treated samples were used to quantify DIMBOA and DIMBOA-Glc. These samples included the T_4 transgenic and non-transgenic (ND101) maize seedlings at 7 days after germination (DAG), as well as inoculated and non-inoculated seedlings at 24 and 48 hai. Root samples were collected and immediately frozen in liquid nitrogen, then stored at −80 °C. The content of DIMBOA and DIMBOA-Glc were quantified using ultra-high pressure liquid chromatography-mass spectrometry, according to previously reported method (Liu *et al*., 2012).

Acknowledgements

We thank Chang Liu and Sureshkumar Balasubramania for critical comments on this manuscript. We thank Daolong Dou for *Pythium aphanidermatum*, Xiaohong Yang for the maize inbred population, Tao Zhou for maize gene VIGS toolkit, Mingliang Xu for pGreenII 0800-LUC vector, and Jinbo Zhang for ZmTPK-GFP plasmid. We thank Pengfei Yin for kind help with data analysis, Yuanliang Liu for help with maize seed breeding, and Linlu Qi for help with DIMBOA and DIMBOA-Glc quantification. This work was supported by the National Key Research and Development Program, Ministry of Science and Technology of China (No. 2022YFD1201802), the Pinduoduo-China Agricultural University Research Fund (Grant No. PC2023A01005), and the 2115 Talent Development Program of China Agricultural University (No. 2020RC013; W.Z.).

Conflict of interest

The authors declare no competing interests.

Author contributions

Conceptualization: C.L., W.Z. Methodology: C.L., S.H., J.C., C.A., J.S. Formal analysis: C.L., S.H., J.C. Investigation: C.L., S.H., J.C., M.W., Z.L., L.W., Y.C., M.D. Writing—original draft: C.L. Writing—review, and editing: W.Z. Supervision: W.Z. Project administration: W.Z. Funding acquisition: W.Z.

Data availability statement

Data sharing not applicable to this article as no datasets were generated or analysed during the current study.

References

Ahmad, S., Veyrat, N., Gordon-Weeks, R., Zhang, Y., Martin, J., Smart, L., Glauser, G. *et al*. (2011) Benzoxazinoid metabolites regulate innate immunity against aphids and fungi in maize. *Plant Physiol.* **157**, 317–327.

Baiya, S., Hua, Y., Ekkhara, W. and Ketudat Cairns, J.R. (2014) Expression and enzymatic properties of rice (*Oryza sativa* L.) monolignol β-glucosidases. *Plant Sci.* **227**, 101–109.

Baiya, S., Mahong, B., Lee, S.-K., Jeon, J.-S. and Ketudat Cairns, J.R. (2018) Demonstration of monolignol β-glucosidase activity of rice Os4BGlu14, Os4BGlu16 and Os4BGlu18 in *Arabidopsis thaliana bglu45* mutant. *Plant Physiol. Biochem.* **127**, 223–230.

Balmer, D., de Papajewski, D.V., Planchamp, C., Glauser, G. and Mauch-Mani, B. (2013) Induced resistance in maize is based on organ-specific defence responses. *Plant J.* **74**, 213–225.

Barros, J., Serk, H., Granlund, I. and Pesquet, E. (2015) The cell biology of lignification in higher plants. *Ann. Bot.* **115**, 1053–1074.

Bhuiyan, N.H., Selvaraj, G., Wei, Y. and King, J. (2009) Gene expression profiling and silencing reveal that monolignol biosynthesis plays a critical role in penetration defence in wheat against powdery mildew invasion. *J. Exp. Bot.* **60**, 509–521.

Bradbury, P.J., Zhang, Z., Kroon, D.E., Casstevens, T.M., Ramdoss, Y. and Buckler, E.S. (2007) TASSEL: software for association mapping of complex traits in diverse samples. *Bioinformatics*, **23**, 2633–2635.

Butrón, A., Chen, Y.C., Rottinghaus, G.E. and McMullen, M.D. (2010) Genetic variation at *bx1* controls DIMBOA content in maize. *Theor. Appl. Genet.* **120**, 721–734.

Cesarino, I. (2019) Structural features and regulation of lignin deposited upon biotic and abiotic stresses. *Curr. Opin. Biotechnol.* **56**, 209–214.

Chávez-Arias, C.C., Ligarreto-Moreno, G.A., Ramírez-Godoy, A. and Restrepo-Díaz, H. (2021) Maize responses challenged by drought, elevated daytime temperature and arthropod herbivory stresses: a physiological, biochemical and molecular view. *Front. Plant Sci.* **12**, 702841.

Chen, R., Yao, Y., Fang, H., Zhang, E., Li, P., Xu, Y., Yin, S. *et al*. (2019) Origin, evolution and functional characterization of the land plant glycoside hydrolase subfamily GH5_11. *Mol. Phylogenet. Evol.* **138**, 205–218.

Chen, J.B., Bao, S.W., Fang, Y.L., Wei, L.Y., Zhu, W.S., Peng, Y.L. and Fan, J. (2021) An LRR-only protein promotes NLP-triggered cell death and disease susceptibility by facilitating oligomerization of NLP in Arabidopsis. *New Phytol.* **232**, 1808–1822.

Cheng, W., Hong, C., Zeng, F., Liu, N. and Gao, H. (2023) Sequence variations affect the 5′ splice site selection of plant introns. *Plant Physiol.* **375**, 1281–1296.

Christensen, S.A., Huffaker, A., Sims, J., Hunter, C.T., Block, A., Vaughan, M.M., Willett, D. *et al*. (2018) Fungal and herbivore elicitation of the novel maize sesquiterpenoid, zealexin A4, is attenuated by elevated CO_2. *Planta*, **247**, 863–873.

Degenhardt, J., Hiltpold, I., Köllner, T.G., Frey, M., Gierl, A., Gershenzon, J., Hibbard, B.E. *et al*. (2009) Restoring a maize root signal that attracts insect-killing nematodes to control a major pest. *Proc. Natl Acad. Sci. USA*, **106**, 13213–13218.

Dent, C.I., Singh, S., Mukherjee, S., Mishra, S., Sarwade, R.D., Shamaya, N., Loo, K.P. *et al*. (2021) Quantifying splice-site usage: a simple yet powerful approach to analyze splicing. *NAR Genom Bioinform.* **3**, lqab041.

Diezel, C., Kessler, D. and Baldwin, I.T. (2011) Pithy protection: nicotiana attenuata's jasmonic acid-mediated defenses are required to resist stem-boring weevil larvae. *Plant Physiol.* **155**, 1936–1946.

Ding, X.S., Schneider, W.L., Chaluvadi, S.R., Mian, M.A.R. and Nelson, R.S. (2006) Characterization of a Brome mosaic virus strain and its use as a vector for gene silencing in monocotyledonous hosts. *Mol. Plant Microbe Interact.* **19**, 1229–1239.

Ding, Y., Murphy, K.M., Poretsky, E., Mafu, S., Yang, B., Char, S.N., Christensen, S.A. *et al*. (2019) Multiple genes recruited from hormone pathways partition maize diterpenoid defences. *Nat. Plants*, **5**, 1043–1056.

Duan, C.X., Song, F.J., Sun, S.L., Guo, C., Zhu, Z.D. and Wang, X.M. (2019) Characterization and molecular mapping of two novel genes resistant to Pythium stalk rot in maize. *Phytopathology*, **109**, 804–809.

Fia, G., Giovani, G. and Rosi, I. (2005) Study of beta-glucosidase production by wine-related yeasts during alcoholic fermentation. A new rapid fluorimetric method to determine enzymatic activity. *J. Appl. Microbiol.* **99**, 509–517.

Filichkin, S., Priest, H.D., Megraw, M. and Mockler, T.C. (2015) Alternative splicing in plants: directing traffic at the crossroads of adaptation and environmental stress. *Curr. Opin. Plant Biol.* **24**, 125–135.

Fu, J., Ren, F., Lu, X., Mao, H., Xu, M. and Degenhardt, J. (2016) A tandem array of ent-kaurene synthases in maize with roles in gibberellin and more specialized metabolism. *Plant*, **170**, 742–751.

Glauser, G., Marti, G., Villard, N., Doyen, G.A., Wolfender, J.-L., Turlings, T.C.J. and Erb, M. (2011) Induction and detoxification of maize 1,4-benzoxazin-3-ones by insect herbivores. *Plant J.* **68**, 901–911.

Gómez-Anduro, G., Ceniceros-Ojeda, E.A., Casados-Vázquez, L.E., Bencivenni, C., Sierra-Beltrán, A., Murillo-Amador, B. and Tiessen, A. (2011) Genome-wide analysis of the beta-glucosidase gene family in maize (*Zea mays* L. var B73). *Plant Mol. Biol.* **77**, 159–183.

Gorman, Z., Christensen, S.A., Yan, Y., He, Y., Borrego, E. and Kolomiets, M.V. (2020) Green leaf volatiles and jasmonic acid enhance susceptibility to anthracnose diseases caused by *Colletotrichum graminicola* in maize. *Mol. Plant Pathol.* **21**, 702–715.

Guo, J., Qi, J., He, K., Wu, J., Bai, S., Zhang, T., Zhao, J. *et al*. (2019) The Asian corn borer Ostrinia furnacalis feeding increases the direct and indirect defence of mid-whorl stage commercial maize in the field. *Plant Biotechnol. J.* **17**, 88–102.

Guo, M., Zhang, Y., Jia, X., Wang, X., Zhang, Y., Liu, J., Yang, Q. *et al*. (2022) Alternative splicing of *REGULATOR OF LEAF INCLINATION 1* modulates phosphate starvation signaling and growth in plants. *Plant Cell*, **34**, 3319–3338.

Hanemian, M., Vasseur, F., Marchadier, E., Gilbault, E., Bresson, J., Gy, I., Violle, C. *et al*. (2020) Natural variation at *FLM* splicing has pleiotropic effects modulating ecological strategies in *Arabidopsis thaliana*. *Nat. Commun.* **11**, 4140.

Huffaker, A., Pearce, G., Veyrat, N., Erb, M., Turlings, T.C.J., Sartor, R., Shen, Z. *et al*. (2013) Plant elicitor peptides are conserved signals regulating direct and indirect antiherbivore defense. *Proc. Natl Acad. Sci. USA*, **110**, 5707–5712.

Joo, Y., Kim, H., Kang, M., Lee, G., Choung, S., Kaur, H., Oh, S. *et al*. (2021) Pith-specific lignification in *Nicotiana attenuata* as a defense against a stem-boring herbivore. *New Phytol.* **232**, 332–344.

Ketudat Cairns, J.R. and Esen, A. (2010) β-Glucosidases. *Cell. Mol. Life Sci.* **67**, 3389–3405.

Ketudat Cairns, J.R., Mahong, B., Baiya, S. and Jeon, J.S. (2015) β-Glucosidases: multitasking, moonlighting or simply misunderstood? *Plant Sci.* **241**, 246–259.

Khokhar, M.K., Hooda, K.S., Sharma, S.S. and Singh, V. (2014) Post flowering stalk rot complex of maize-present status and future prospects. *Maydica*, **59**, 226–242.

Kondo, Y., Oubridge, C., van Roon, A.-M.M. and Nagai, K. (2015) Crystal structure of human U1 snRNP, a small nuclear ribonucleoprotein particle, reveals the mechanism of 5′ splice site recognition. *Elife*, **4**, e04986.

Kong, W., Zhong, H., Deng, X., Gautam, M., Gong, Z., Zhang, Y., Zhao, G. *et al*. (2019) Evolutionary analysis of *GH3* genes in six *Oryza* species/subspecies and their expression under salinity stress in *Oryza sativa* ssp. *japonica*. *Plan. Theory*, **8**, 30.

Laloum, T., Martín, G. and Duque, P. (2018) Alternative splicing control of abiotic stress responses. *Trends Plant Sci.* **23**, 140–150.

Lam, P.Y., Wang, L., Lo, C. and Zhu, F.Y. (2022) Alternative splicing and its roles in plant metabolism. *Int. J. Mol. Sci.* **23**, 7355.

Lee, M.H., Jeon, H.S., Kim, S.H., Chung, J.H., Roppolo, D., Lee, H.J., Cho, H.J. *et al*. (2019) Lignin-based barrier restricts pathogens to the infection site and confers resistance in plants. *EMBO J.* **38**, e101948.

Li, Y.I., van de Geijn, B., Raj, A., Knowles, D.A., Petti, A.A., Golan, D., Gilad, Y. *et al*. (2016) RNA splicing is a primary link between genetic variation and disease. *Science*, **352**, 600–604.

Liu, C.J., Miao, Y.C. and Zhang, K.W. (2011) Sequestration and transport of lignin monomeric precursors. *Molecules*, **16**, 710–727.

Liu, H., Li, X., Xiao, J. and Wang, S. (2012) A convenient method for simultaneous quantification of multiple phytohormones and metabolites: application in study of rice-bacterium interaction. *Plant Methods*, **8**, 2.

Livak, K.J. and Schmittgen, T.D. (2001) Analysis of relative gene expression data using real-time quantitative PCR and the 2(-Delta Delta C(T)) method. *Methods*, **25**, 402–408.

Maag, D., Köhler, A., Robert, C.A., Frey, M., Wolfender, J.L., Turlings, T.C. *et al*. (2016) Highly localized and persistent induction of *Bx1*-dependent herbivore resistance factors in maize. *Plant J.* **88**, 976–991.

Mafu, S., Ding, Y., Murphy, K.M., Yaacoobi, O., Addison, J.B., Wang, Q., Shen, Z. *et al*. (2018) Discovery, biosynthesis and stress-related accumulation of dolabradiene-derived defenses in maize. *Plant Physiol.* **176**, 2677–2690.

Mahuku, G. (2010) Maize pathology in Asia: opportunities and challenges for breeding disease-resistant maize. *Proc. Asian Reg. Maize Workshop.* **10**, 361–366.

Makowska, B., Bakera, B. and Rakoczy-Trojanowska, M. (2015) The genetic background of benzoxazinoid biosynthesis in cereals. *Acta Physiol. Plant.* **37**, 176.

Malinovsky, F.G., Fangel, J.U. and Willats, W.G.T. (2014) The role of the cell wall in plant immunity. *Front. Plant Sci.* **5**, 178.

Mandadi, K.K., Petrillo, E., Dubrovina, A.S. and Kiselev, K.V. (2023) Editorial: Regulation of alternative splicing in plant stress responses. *Front. Plant Sci.* **13**, 1120961.

Meihls, L.N., Handrick, V., Glauser, G., Barbier, H., Kaur, H., Haribal, M.M., Lipka, A.E. *et al*. (2013) Natural variation in maize aphid resistance is associated with 2,4-dihydroxy-7-methoxy-1,4-benzoxazin-3-one glucoside methyltransferase activity. *Plant Cell*, **25**, 2341–2355.

Minic, Z. and Jouanin, L. (2006) Plant glycoside hydrolases involved in cell wall polysaccharide degradation. *Plant Physiol. Biochem.* **44**, 435–449.

Moreira, X. and Abdala-Roberts, L. (2018) Interactions between plant defence signalling pathways: evidence from bioassays with insect herbivores and plant pathogens. *J. Ecol.* **106**, 2353–2364.

Munkvold, G.P. and White, D.G. (2016) *Compendium of Corn Diseases*, 4nd edn. USA: The American Phytopathological Society. https://doi.org/10.1094/9780890544945.fm

Ninkuu, V., Yan, J., Fu, Z., Yang, T., Ziemah, J., Ullrich, M.S., Kuhnert, N. *et al*. (2022) Lignin and its pathway-associated phytoalexins modulate plant defense against fungi. *J. Fungi*, **9**, 52.

Ohno, K., Takeda, J.-I. and Masuda, A. (2018) Rules and tools to predict the splicing effects of exonic and intronic mutations. *Wiley Interdiscip. Rev. RNA*, **9**, e1451.

Perkins, M., Smith, R.A. and Samuels, L. (2019) The transport of monomers during lignification in plants: anything goes but how? *Curr. Opin. Biotechnol.* **56**, 69–74.

Quentin, M., Allasia, V., Pegard, A., Allais, F., Ducrot, P.-H., Favery, B., Levis, C. *et al*. (2009) Imbalanced lignin biosynthesis promotes the sexual reproduction of homothallic oomycete pathogens. *PLoS Pathog.* **5**, e1000264.

Ren, R.J., Wang, P., Wang, L.N., Su, J.P., Sun, L.J., Sun, Y., Chen, D.F. *et al*. (2020) Os4BGlu14, a monolignol β-Glucosidase, negatively affects seed longevity by influencing primary metabolism in rice. *Plant Mol. Biol.* **104**, 513–527.

Salz, H.K. (2011) Sex determination in insects: a binary decision based on alternative splicing. *Curr. Opin. Genet. Dev.* **21**, 395–400.

Sattler, S.E. and Funnell-Harris, D.L. (2013) Modifying lignin to improve bioenergy feedstocks: strengthening the barrier against pathogens? *Front. Plant Sci.* **4**, 70.

Sha, G., Sun, P., Kong, X., Han, X., Sun, Q., Fouillen, L., Zhao, J. *et al*. (2023) Genome editing of a rice CDP-DAG synthase confers multipathogen resistance. *Nature*, **618**, 1–7.

Song, F.J., Xiao, M.G., Duan, C.X., Li, H.J., Zhu, Z.D., Liu, B.T., Sun, S.L. *et al*. (2015) Two genes conferring resistance to Pythium stalk rot in maize inbred line Qi319. *Mol. Genet. Genomics*, **290**, 1543–1549.

Sun, Q., Liu, X., Yang, J., Liu, W., Du, Q., Wang, H. *et al*. (2018) MicroRNA528 affects lodging resistance of maize by regulating lignin biosynthesis under nitrogen-luxury conditions. *Mol. Plant*, **11**, 806–814.

Tang, R.J., Zhao, F.G., Yang, Y., Wang, C., Li, K., Kleist, T.J. *et al*. (2020) A calcium signaling network activates vacuolar K+ remobilization to enable plant adaptation to low-K environments. *Nat. Plants*, **6**, 284–393.

Tronchet, M., Balagué, C., Kroj, T., Jouanin, L. and Roby, D. (2010) Cinnamyl alcohol dehydrogenases-C and D, key enzymes in lignin biosynthesis, play an essential role in disease resistance in Arabidopsis. *Mol. Plant Pathol.* **11**, 83–92.

Tzin, V., Lindsay, P.L., Christensen, S.A., Meihls, L.N., Blue, L.B. and Jander, G. (2015) Genetic mapping shows intraspecific variation and transgressive segregation for caterpillar-induced aphid resistance in maize. *Mol. Ecol.* **24**, 5739–5750.

Vanholme, R., Demedts, B., Morreel, K., Ralph, J. and Boerjan, W. (2010) Lignin biosynthesis and structure. *Plant Physiol.* **153**, 895–905.

Vaughan, M.M., Block, A., Christensen, S.A., Allen, L.H. and Schmelz, E.A. (2018) The effects of climate change associated abiotic stresses on maize phytochemical defenses. *Phytochem. Rev.* **17**, 37–49.

Veronico, P., Paciolla, C., Pomar, F., De Leonardis, S., García-Ulloa, A. and Melillo, M.T. (2018) Changes in lignin biosynthesis and monomer composition in response to benzothiadiazole and root-knot nematode *Meloidogyne incognita* infection in tomato. *J. Plant Physiol.* **230**, 40–50.

Wang, R., Yang, X., Wang, N., Liu, X., Nelson, R.S., Li, W., Fan, Z. *et al*. (2016) An efficient virus-induced gene silencing vector for maize functional genomics research. *Plant J.* **86**, 102–115.

Wang, C., Yang, Q., Wang, W., Li, Y., Guo, Y., Zhang, D., Ma, X. *et al*. (2017) A transposon-directed epigenetic change in *ZmCCT* underlies quantitative resistance to *Gibberella* stalk rot in maize. *New Phytol.* **215**, 1503–1515.

Wang, X., Yang, M., Ren, D., Terzaghi, W., Deng, X.-W. and He, G. (2019) Cis-regulated alternative splicing divergence and its potential contribution to environmental responses in Arabidopsis. *Plant J.* **97**, 555–570.

Wang, C., Chen, S., Dong, Y., Ren, R., Chen, D. and Chen, X. (2020) Chloroplastic Os3BGlu6 contributes significantly to cellular ABA pools and impacts drought tolerance and photosynthesis in rice. *New Phytol.* **226**, 1042–1054.

Wei, T., Tang, Y., Jia, P., Zeng, Y., Wang, B., Wu, P., Quan, Y. *et al*. (2021) A cotton lignin biosynthesis gene, *GhLAC4*, fine-tuned by ghr-miR397 modulates plant resistance against *Verticillium dahliae*. *Front. Plant Sci.* **12**, 743795.

Xu, X., Yang, D., Ding, J.-H., Wang, W., Chu, P.-H., Dalton, N.D., Wang, H.Y. *et al*. (2005) ASF/SF2-regulated CaMKIIdelta alternative splicing temporally reprograms excitation-contraction coupling in cardiac muscle. *Cell*, **120**, 59–72.

Xu, J., Wang, X., Zu, H., Zeng, X., Baldwin, I.T. and Lou, Y. (2021) Molecular dissection of rice phytohormone signaling involved in resistance to a piercing-sucking herbivore. *New Phytol.* **230**, 1639–1652.

Yang, D.E., Zhang, C.L. and Wang, Y.G. (2002) Review of maize stalk rot in China. *J. Maize Sci.* **10**, 88–90.

Yang, Q., Yin, G.M., Guo, Y.L., Zhang, D.F., Chen, S.J. and Xu, M.L. (2010) A major QTL for resistance to *Gibberella* stalk rot in maize. *Theor. Appl. Genet.* **121**, 673–687.

Yang, Q., Li, Z., Li, W., Ku, L., Wang, C., Ye, J., Li, K. *et al*. (2013) CACTA-like transposable element in *ZmCCT* attenuated photoperiod sensitivity and accelerated the postdomestication spread of maize. *Proc. Natl Acad. Sci. USA*, **110**, 16969–16974.

Ye, J., Zhong, T., Zhang, D., Ma, C., Wang, L., Yao, L., Zhang, Q. *et al*. (2019) The auxin-regulated protein ZmAuxRP1 coordinates the balance between root growth and stalk rot disease resistance in maize. *Mol. Plant*, **12**, 360–373.

Yuan, C., Li, C., Yan, L., Jackson, A.O., Liu, Z., Han, C., Yu, J. *et al*. (2011) A high throughput barley stripe mosaic virus vector for virus induced gene silencing in monocots and dicots. *PloS One*, **6**, e26468.

Yuan, W., Jiang, T., Du, K., Chen, H., Cao, Y., Xie, J. *et al*. (2019) Maize phenylalanine ammonia-lyases contribute to resistance to Sugarcane mosaic virus infection, most likely through positive regulation of salicylic acid accumulation. *Mol. Plant Pathol.* **20**, 1365–1378.

Zagrobelny, M., Bak, S. and Møller, B.L. (2008) Cyanogenesis in plants and arthropods. *Phytochemistry*, **69**, 1457–1468.

Zhang, C., Li, J., Li, S., Ma, C., Liu, H., Wang, L., Qi, J. *et al*. (2021) ZmMPK6 and ethylene signalling negatively regulate the accumulation of anti-insect metabolites DIMBOA and DIMBOA-Glc in maize inbred line A188. *New Phytol.* **229**, 2273–2287.

Zhou, C., Li, D., Shi, X., Zhang, J., An, Q., Wu, Y., Kang, L. *et al*. (2021) Nanoselenium enhanced wheat resistance to aphids by regulating biosynthesis of DIMBOA and volatile components. *J. Agric. Food Chem.* **69**, 14103–14114.

Yang, X.H., Gao, S.B., Xu, S.T., Zhang, Z.X., Prasanna, B.M., Li, L., Li, J.S. *et al*. (2011) Characterization of a global germplasm collection and its potential utilization for analysis of complex quantitative traits in maize. *Molecular Breeding*, **28**, 511–526.

Supporting information

Additional supporting information may be found online in the Supporting Information section at the end of the article.

Figures S1-S7 Figure S1 (a) Histogram of the frequency distribution of root disease severity index in 189 lines of maize inoculated with *P. aphanidermatum*. (b) The quantile-quantile (Q–Q) plot, which demonstrated the overlapped and exceeded associations between the observed signals and the expected signals under the null hypotheses.

Figure S2 Comparison of the GEMS10 and TY4 of *ZmBGLU17* CDS sequences. Identical bases are highlighted in black.

Figure S3 Sequences comparison of the amino acid of different transcripts of ZmBGLU17 between GEMS10 and TY4.

Figure S4 Natural variation in +4 position of the fifth intron splicing site in certain ecotypes.

Figure S5 The natural variation of the signal peptide in *ZmBGLU17* does not affect its secretion to the extracellular matrix.

Figure S6 Phenotypic analysis of yield in F_2 populations with different resistance and susceptible haplotypes.

Figure S7 The relative β-D glucosidase enzymatic activity of ZmGlu1 and ZmGlu2.

Table S1 189 maize inbred lines and their average disease severity score.

Table S2 The information for the 43 SNPs.

Table S3 Oligonucleotide primers.

